Author Manuscript

Author Manuscript

Author Manuscript

Author Manuscript

HHS Public Access

Author manuscript

Cell Rep. Author manuscript; available in PMC 2019 February 12.

Published in final edited form as:

Cell Rep. 2018 November 27; 25(9): 2417–2430.e5. doi:10.1016/j.celrep.2018.10.097.

Esrp1-Regulated Splicing of Arhgef11 Isoforms Is Required for Epithelial Tight Junction Integrity

SungKyoung Lee[1], **Benjamin Cieply**[1], **Yueqin Yang**[1], **Natoya Peart**[1], **Carl Glaser**[1], **Patricia Chan**[1], and **Russ P. Carstens**[1,2,3,*]

[1]Department of Medicine, Perelman School of Medicine, University of Pennsylvania, Philadelphia, PA 19104, USA

[2]Department of Genetics, Perelman School of Medicine, University of Pennsylvania, Philadelphia, PA 19104, USA

[3]Lead Contact

SUMMARY

The epithelial-specific splicing regulators Esrp1 and Esrp2 are required for mammalian development, including establishment of epidermal barrier functions. However, the mechanisms by which Esrp ablation causes defects in epithelial barriers remain undefined. We determined that the ablation of *Esrp1* and *Esrp2* impairs epithelial tight junction (TJ) integrity through loss of the epithelial isoform of Rho GTP exchange factor Arhgef11. Arhgef11 is required for the maintenance of TJs via RhoA activation and myosin light chain (MLC) phosphorylation. Ablation or depletion of *Esrp1/2* or *Arhgef11* inhibits MLC phosphorylation and only the epithelial Arhgef11 isoform rescues MLC phosphorylation in *Arhgef11* KO epithelial cells. Mesenchymal Arhgef11 transcripts contain a C-terminal exon that binds to PAK4 and inhibits RhoA activation byArhgef11. Deletion of the mesenchymal-specific *Arhgef11* exon in Esrp1/2 KO epithelial cells using CRISPR/Cas9 restored TJ function, illustrating how splicing alterations can be mechanistically linked to disease phenotypes that result from impaired functions of splicing regulators.

Graphical Abstract

This is an open access article under the CC BY-NC-ND license (http://creativecommons.org/licenses/by-nc-nd/4.0/).

*Correspondence: russcars@upenn.edu.

AUTHOR CONTRIBUTIONS

S.K.L. performed most of the experiments. B.C., Y.Y., N.P., P.C., and C.G. performed some experiments and contributed to manuscript preparation. R.P.C. and S.K.L. conceived and designed the study and wrote the manuscript.

SUPPLEMENTAL INFORMATION

Supplemental Information includes six figures and three tables and can be found with this article online at https://doi.org/10.1016/j.celrep.2018.10.097.

DECLARATION OF INTERESTS

The authors declare no competing interests.

Author Manuscript Author Manuscript Author Manuscript Author Manuscript

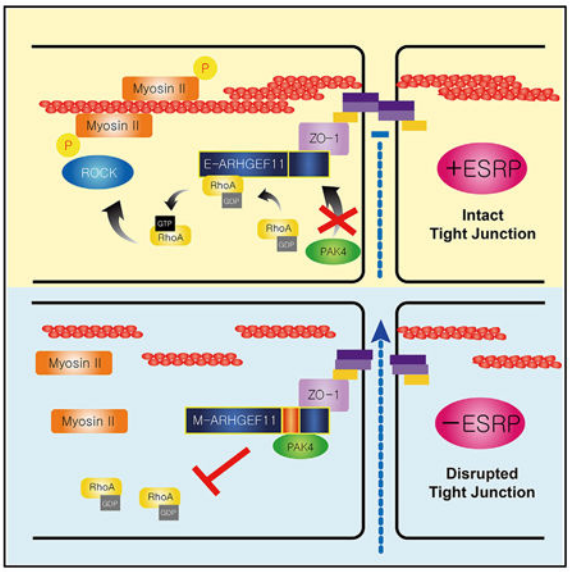

In Brief

Lee et al. identify defects in epithelial tight junctions when the splicing regulators *Esrp1* and *Esrp2* are ablated in mouse epidermis. A splicing switch in *Arhgef11* transcripts partially underlies these defects through inhibition of the mesenchymal isoform of Arhgef11 by Pak4 and a consequent loss of RhoA activation.

INTRODUCTION

Alternative splicing (AS) is a highly regulated process of gene expression that results in the production of multiple protein isoforms from a single gene. Nearly all human (>90%) pre-mRNA transcripts undergo AS, with an average of 7–8 AS events per multi-exon gene (Pan et al., 2008; Wang et al., 2008). While recent studies strongly suggest that a large number of AS events lead to alternative protein isoforms, for the vast majority of alternatively spliced transcripts, the functional consequences of AS at the level of protein function remain unknown (Blencowe, 2017). Dysregulation of AS has been shown to lead to numerous human diseases, and thus a better understanding of how inappropriate expression of specific protein isoforms can be associated with specific disease phenotypes is needed (Cieply and Carstens, 2015; Shkreta and Chabot, 2015). However, associating global changes in splicing with the functions of specific cell types or with relevant disease phenotypes remains a major challenge because defining the biological function of even a single AS event can require years of detailed study (Blencowe, 2017). Recent studies have demonstrated that a major impact of AS at the protein level is to alter protein-protein interactions. Alternatively spliced exons encode protein regions that are highly enriched for regions of protein disorder and post-translational modifications, both of which are associated with protein-protein interactions (Buljan et al., 2012; Ellis et al., 2012). Alternative exons with cell- or tissue-specific splicing differences are even more highly enriched for these features, indicating that a major function of tissue-specific AS is to “rewire” protein-protein interaction networks in different cell types to globally affect differential cell functions and properties. A recent

Author Manuscript Author Manuscript Author Manuscript Author Manuscript

large-scale study that examined protein-protein interactions for a panel of alternative isoform pairs confirmed these observations and revealed that AS produces isoforms with vastly different interaction profiles, such that different isoforms often behave as if they arise from completely different genes (Yang et al., 2016a). Therefore, alternatively spliced protein isoforms tend to behave like distinct genes in interactome networks rather than minor variants. A first step toward resolving the functional consequences of AS can begin with the identification of isoform-specific protein interactions, followed by a more detailed analysis of how these altered protein interactions mechanistically affect complexes and pathways that are important for specific cell operations.

AS is largely regulated by RNA-binding proteins (RBPs) that function as splicing factors, including a growing list of these factors with cell- or tissue-specific expression (Chen and Manley, 2009). The epithelial splicing regulatory proteins 1 (ESRP1) and 2 (ESRP2) are exquisitely epithelial cell type-specific splicing factors that regulate a large network of alternatively spliced genes involved in cell-cell adhesion, motility, cytoskeletal dynamics, and epithelial-to-mesenchymal transition (EMT) (Dittmar et al., 2012; Warzecha et al., 2009, 2010; Yang et al., 2016b). We previously generated mice with germline and/or conditional knockout alleles for *Esrp1* and *Esrp2* and showed that they are essential for mammalian development, with important roles in the formation of multiple organs or structures (Bebee et al., 2015). More recently, we also showed that mutations in *ESRP1* lead to human hereditary sensorineural hearing loss through structural alterations of the inner ear that mirror those seen in *Esrp1* knockout (KO) mouse ears during development (Rohacek et al., 2017). In addition, conditional ablation of *Esrp1* and *Esrp2* in the epidermis demonstrated that loss of *Esrp1* and *Esrp2* in the epidermis was postnatal lethal due to excessive water loss and dehydration (Bebee et al., 2015).

The epidermal cells of the skin constitute one of the most important populations of epithelial cells in mammals because the skin provides an essential barrier that acts as the first line of defense protecting the human body against outside environmental and microbial threats. Furthermore, through the formation of the epidermal permeability barrier (EPB), the epidermis limits the flow of water, ions, and other small molecules across epithelial cell layers and prevents water loss and dehydration (Kirschner and Brandner, 2012). Thus, maintenance of the EPB is crucial for survival, and defects in EPB are associated with a number of skin diseases, including inflammatory skin diseases such as atopic dermatitis and psoriasis (Kubo et al., 2012). It is therefore of great relevance to understand the basis of defects in EPB formation and function to identify new therapeutic strategies. Our discovery of a defect in the EPB in Esrp-ablated skin suggested that splicing switches in key Esrp splicing targets underlie this abnormality. The identification of some of these events holds the potential for identifying genes and splice isoform-dependent pathways that are essential for barrier functions in the epidermis, as well as in other epithelial cells that form important cell barriers in other organs such as the gastrointestinal tract and lungs.

The epithelial cells that comprise the epidermis consist of several stratified layers of keratinocytes. The basal layer, or stratum basale, contains epithelial cells abutting the basement membrane and dermis. As these cells differentiate and migrate upward, they give rise to the stratum spinosum, stratum granulosum, and finally the stratum corneum, which

Author Manuscript Author Manuscript Author Manuscript Author Manuscript

consists of dead corneocytes and lipids that constitute the outermost layer of the skin barrier (Kirschner and Brandner, 2012). Previous studies demonstrated that tight junctions (TJs), located at the stratum granulosum of skin, play an essential role in the maintenance of the EPB to prevent water loss (Furuse et al., 2002; Tunggal et al., 2005). Our previous identification of genes with AS changes in *Esrp1*;*Esrp2* double KO (DKO) epidermis revealed enrichment for transcripts encoding Kyoto Encyclopedia of Genes and Genomes (KEGG) category "Tight Junction," and we also observed numerous Esrp regulated targets that are associated with and/or involved in the functions of TJs, suggesting that these structures were disrupted in Esrp ablated epidermis. Here, we characterize TJ defects in Esrp ablated epithelial cells *in vivo* and *in vitro* and describe a molecular mechanism through which a splicing switch in *Arhgef11* transcripts partially underlies these defects.

RESULTS

Esrp1 and *Esrp2* Are Required for Structural TJ Integrity *In Vivo* and *In Vitro*

Our previous observation of dry skin and lethal water loss in newborn pups after conditional *Esrp1;Esrp2* ablation in the epidermis prompted further inquiry into the etiology of this barrier defect. TJs are composed of two groups of proteins. Adaptor proteins (e.g., ZO-1) connect the cytoskeleton to the junctional membrane and provide protein-protein interaction through scaffolding function. The transmembrane proteins (Occludin and Claudins) link these adaptor proteins and mediate cell-cell adhesion (Zihni et al., 2016). We performed immunofluorescence for TJ proteins in *Esrp1*$^{+/+}$;*Esrp2*$^{-/-}$ controls and Esrp DKO (*Esrp1*$^{-/-}$;*Esrp2*$^{-/-}$) littermates at embryonic day (E)18.5. Occludin specifically stains at the granular cell layer where the TJs are located. We noted the expected pattern of continuous linear staining for Occludin in control embryos, whereas in DKO epidermis we noted discontinuous staining, suggesting areas of disrupted TJs (Figure 1A). ZO-1 and Claudin-4 staining was observed throughout the epidermal layers, as noted in previous studies (Furuse et al., 2002), and while staining for ZO-1 appeared slightly discontinuous, these stains primarily showed a reduced thickness of the hypoplastic epidermis, as originally observed on H&E staining (Bebee et al., 2015) (Figures 1B and 1C). Of note, we used *Esrp1*$^{+/+}$;*Esrp2*$^{-/-}$ embryos as controls from the same litters as *Esrp1*$^{-/-}$;*Esrp2*$^{-/-}$ embryos because Esrp1 and Esrp2 are both highly expressed in the epidermis and *Esrp2*$^{-/-}$ mice have no observable phenotypes (Bebee et al., 2015). Moreover, epidermis from *Esrp2*$^{-/-}$ mice displays no histologic abnormalities or defects in Occludin staining in *Esrp2*$^{-/-}$ epidermis compared to wild-type epidermis (Figures S1A and S1B). Next, to examine whether Esrp1 is required for TJ structural formation *in vitro*, we examined ZO-1 and Occludin immunofluorescence following calcium-induced TJ assembly in cells, which followed short hairpin RNA (shRNA)-mediated *Esrp1* and *Esrp2* depletion (double knockdown [DKD]) compared to non-targeting shRNA controls (Con) in the mouse MKC-6 keratinocyte cell line. Whereas control cells showed continuous staining along cell junctions, these TJ markers were disrupted following *Esrp1* and *Esrp2* depletion and showed increased diffuse localization throughout the cytoplasm (Figure 1D). These data demonstrate that the Esrps are essential for structural integrity at cell-cell junctions *in vivo* and *in vitro*.

Author Manuscript Author Manuscript Author Manuscript Author Manuscript

Ablation or Depletion of the Esrps Results in Increased Permeability through TJs

The water loss phenotype and alterations in TJ markers in *Esrp1*$^{-/-}$;*Esrp2*$^{-/-}$ pups suggested an "inside-out" permeability defect similar to other mouse models associated with defective TJs (Furuse et al., 2002; Gladden et al., 2010; Tunggal et al., 2005). To further establish that the water loss in *Esrp1*$^{-/-}$;*Esrp2*$^{-/-}$ DKO epidermis was due to a defect in the TJ-based permeability, we used previously described assays for TJ functional integrity (Schmitz et al., 2015). In normal mouse skin, sulfo-N-Hydroxysuccinimide (NHS)-biotin injected into the dermis will diffuse into the epidermis, but will be halted at the TJs located at the stratum granulosum (marked with Occludin staining) and prevented from leaking into the stratum corneum (Figure 1E). In control E18.5 embryos after labeling biotin with streptavidin, we noted the expected restriction of diffusion across TJs labeled with Occludin. In *Esrp1*$^{-/-}$;*Esrp2*$^{-/-}$ DKO epidermis, we observed that biotin was able to diffuse across the granular cell layer into the stratum corneum, indicating a permeability defect at the level of epidermal TJs (Schmitz et al., 2015) Figure 1F). The stratum corneum comprises another component of the epidermal barrier that is commonly associated with an "outside-in" barrier function to protect against pathogens and chemical insults. The toluidine blue penetration assay is commonly used to identify outside-in permeability defects that are presumed to arise from defects in the function of the stratum corneum (Schmitz et al., 2015). We did not observe differences in toluidine penetration between control and *Esrp1*$^{-/-}$;*Esrp2*$^{-/-}$ DKO embryos, suggesting that the stratum corneum in Esrp-ablated skin was intact in forming the outside-in barrier, similar to previous observations in E-cadherin KO skin that also showed defective TJs (Tunggal et al., 2005) (Figure S1C).

In cultured monolayer cells *in vitro* transepithelial electrical resistance (TEER) and fluorescein isothiocyanate (FITC)-dextran flux assays are commonly used to assess TJ functions to restrict paracellular passage of water, ions, and other small molecules after calcium-induced TJ assembly (Yuki et al., 2007). We measured TEER across confluent cell cultures after control, *Esrp1*-, *Esrp2*-, or *Esrp1/2*-specific shRNA knockdown using mouse MKC-6 keratinocyte cell monolayers that had been stimulated with calcium. Control keratinocytes developed a progressive increase in electrical resistance after calcium stimulation. Whereas *Esrp2* knockdown (KD) cells showed a negligible decrease in TEER, KD of either *Esrp1* alone or of *Esrp1* and *Esrp2* caused a profound reduction in TEER across the time course using two different shRNAs against *Esrp1* (Figures 1G and 1H). Similarly, depletion of *Esrp1* or *Esrp1* and *Esrp2* led to an appreciable increase in flux of 4-kDa FITC-dextran across cell monolayers, further indicating defects in monolayer paracellular permeability and barrier function (Figures 1G and 1H).

Inducible Ablation of the Esrps Postnatally Is Associated with Altered TJs, Inflammation, and Hair Loss

To identify possible defects in epidermal barrier function in adult skin, we used *Esrp1*$^{f/f}$; *K5-rtTA;Esrp2*$^{-/-}$;*tetO-Cre* mice to induce *Esrp* ablation postnatally. We induced *Esrp* ablation by providing doxycycline chow to nursing mothers and subsequently maintained weaned mice with doxycycline chow to maintain *Esrp* ablation. Initially, *Esrp1*$^{f/f}$; *K5-rtTA;Esrp2*$^{-/-}$mice without *tetO-Cre* were used as controls. Adult *Esrp* DKO mice showed variable degrees of hair loss starting at 2 months, as well as variable degrees of

Author Manuscript Author Manuscript Author Manuscript Author Manuscript

inflammatory skin lesions on the back skin (Figure S2A) and weight loss (data not shown). TJ marker ZO-1 and Occludin staining revealed that inducible Esrp DKO (*Esrp1*$^{f/f}$*; K5-rtTA;tetO-Cre;Esrp2*$^{-/-}$) mice consistently also have altered TJ morphology (Figure 2A). Common inflammatory skin disorders, such as and psoriasis and atopic dermatitis, have been associated with the epidermal TJ defects and characterized by epidermal hyperplasia, hyperproliferation in epidermal keratinocytes, and pronounced infiltration of inflammatory cells (De Benedetto et al., 2011; Kirschner and Brandner, 2012). To further explore postnatal Esrp function in epidermal barrier function, we histologically examined *Esrp1*$^{f/f}$*; K5-rtTA; tetO-Cre;Esrp2*$^{-/-}$ DKO skin. These mice showed epidermal hyperplasia and altered morphology of the underlying dermis that resembled fibrosis histologically when analyzed at 3 or 5 months of age (Figure 2B). We noted that Ki-67^{+} cells were increased in epidermal keratinocytes from DKO epidermis compared to controls, indicating increased keratinocyte proliferation (Figure 2C). We did not observe any overt differences in cleaved caspase-3^{+} cells in the DKO epidermis compared to controls, indicating no significant apoptosis in DKO skin (data not shown). Masson's trichrome staining revealed altered patterns of collagen deposition in the dermis that was also consistent with fibrosis and scarring as commonly observed with defects in the epidermal barrier and inflammation in other mouse models (Augustin et al., 2013; Sevilla et al., 2013; Yang et al., 2010) (Figure 2D). To further control for Cre toxicity, leakiness, and doxycycline effects, we also examined the epidermis in *Esrp1*$^{f/f}$*;K5-rtTA;tetO-Cre;Esrp2*$^{-}$ mice that were not given doxycycline and *Esrp1*$^{f/+}$; *K5-rtTA; tetO-Cre;Esrp2*$^{-/-}$ mice that were given doxycycline; neither displayed visual or histologic abnormalities of the skin or hair, indicating that the defects observed were due to *Esrp* ablation (Figures S2B and S2C).

Disrupted TJ barriers have been associated with antigen penetration into the dermis, causing immune system activation and inflammation (Kubo et al., 2012). Antigen exposure activates immune cells such as mast cells, macrophages, neutrophils, and T cells (Pasparakis et al., 2014). We observed increased populations of activated mast cells in Esrp DKO dermis based on toluidine staining (Figure 2E). There was also a notable increase in CD3^{+} cells in the Esrp DKO dermis as well as epidermis (Figure 2F), indicating that the epidermal barrier defect associated with Esrp ablation leads to T cell infiltration. We did not observe differences in macrophage numbers in DKO skin based on F4/80 staining (data not shown). Thus, although Esrp ablation following epidermal differentiation is not lethal, it is associated with altered TJ function and progressive inflammation and scarring.

Depletion of Esrps Is Associated with a Reduction in Myosin Light Chain Phosphorylation

Our previous studies identified large-scale changes in AS of Esrp target transcripts that are enriched for functions associated with epithelial development, including TJs. We further noted a number of Esrp-regulated targets that encode proteins that are either associated with components of epithelial TJs or involved in their regulation based on published data (Bebee et al., 2015) (Figure 3A). Arhgef11 was among the Esrp-regulated targets involving exon 37, which is included in mesenchymal cells but skipped in epithelial cells (Itoh et al., 2017; Shapiro et al., 2011). *Esrp* depletion in MKC-6 cells or ablation in the epidermis induces a switch from the epithelial to the mesenchymal Arhgef11 isoform (Bebee et al., 2015; Rohacek et al., 2017) (Figures 3B–3D). ARHGEF11 is a guanine nucleotide exchange factor

Author Manuscript Author Manuscript Author Manuscript Author Manuscript

for RhoA that localizes to the TJ via a direct interaction with the TJ-associated scaffold protein ZO-1 (also known as TJ protein 1 [TJP1]) (Itoh et al., 2012). TJs associate with the actomyosin cytoskeletal structure referred to as the perijunctional actomyosin ring (PJAR), which encircles epithelial cells in a belt-like manner and plays an essential role in maintaining permeability barriers in epithelial cells through the maintenance of adherens junctions and TJs (Ivanov, 2008; Turner, 2000). Through its association with ZO-1, ARHGEF11 induces myosin light chain (MLC) phosphorylation to promote the assembly of TJs and the PJAR (Itoh, 2013). This activity is most likely due to localized RhoA activation as guanosine triphosphate (GTP)-bound RhoA activates the phosphorylation of MLC, which induces actin filaments to form a functional contractile actomyosin ring that is required for epithelial cell TJ integrity (Nusrat et al., 1995). Consistent with an important role of ARHGEF11 in epithelial barrier and TJ function, a substantial reduction in TEER was observed following a calcium shift, when it was depleted in an epithelial cell line (Itoh et al., 2012). We hypothesized that a switch in *Arhgef11* splicing may contribute to the epithelial barrier defect by altering RhoA activation and MLC phosphorylation. We noted that Esrp1 depletion in the MKC-6 keratinocyte cell line induces a reduction in MLC phosphorylation, and the combined depletion of *Esrp1* and *Esrp2* nearly abolished MLC phosphorylation, whereas *Esrp2* depletion alone showed no apparent effect, correlating with the degree to which each depletion induced a splicing switch in Arhgef11 (Figure 3E). These data indicated that the defects in TJ function at epithelial cell barriers of Esrp depleted cells are associated with reduced MLC phosphorylation and suggested that differential functions of Arhgef11 may underlie this defect.

Epithelial Arhgef11 Isoforms Are More Effective in MLC Phosphorylation and Restoration of Epithelial Cell Barriers through More Efficient Activation of RhoA

To further investigate the TJ defects in epithelial cells, we used CRISPR/Cas9 technology to induce complete gene ablations. Due to the technical shortcomings of mouse keratinocytes, we were unable to achieve effective KO in the MKC-6 or other mouse keratinocytes. We therefore used the Py2T mammary epithelial cell line that was amenable to CRISPR/Cas9-mediated gene ablation and that is a viable model system to further investigate the role of Esrps specifically in functions of epithelial TJs (Waldmeier et al., 2012). To carry out a more detailed analysis of the role of Esrps and Arhgef11 in TJ function, we generated Py2T *Esrp1* KO cells, double *Esrp1* and *Esrp2* KO (DKO) cells, and cells with KO of *Arhgef11*. We isolated clones in which we confirmed complete KO of *Esrp1*, *Esrp2*, and *Arhgef11* both by PCR and western immunoblotting (Figures 4A, 4B, and 5A). Similar to our analyses in MKC-6 keratinocytes, we noted that ablation of *Esrp1* alone as well as of *Esrp1* and *Esrp2* impaired barrier function as measured by both TEER and FITC-dextran tracer flux assays (Figures 4D and 4E). These differences in TEER and dextran flux were not due to differences in cell proliferation or density, as we noted no apparent differences in cell numbers between control and *Esrp1;Esrp2* DKO cells once cells reached confluence at 48 hr in the presence of calcium (Figure S3). Immunofluorescence for Occludin and ZO-1 demonstrated disrupted staining of these TJ markers in *Esrp1;Esrp2* DKO cells and relocalization to the cytoplasm as observed in MKC-6 cells after Esrp depletion (Figure 4F). In addition, we confirmed that ablation of *Esrp1* or *Esrp1* and *Esrp2* induced splicing of mesenchymal exon 37 (Figure 4C). *Arhgef11* ablation also impaired TEER, which is

Author Manuscript Author Manuscript Author Manuscript Author Manuscript

consistent with the previous report using small interfering RNAs (siRNAs), and increased FITC-dextran tracer flux (Itoh et al., 2012) (Figures 5B and 5C). Ablation of *Arhgef11* largely abolished MLC phosphorylation, as also previously shown following siRNA-mediated *Arhgef11* depletion (Figure 5D). To explore whether MLC phosphorylation may be differentially affected by the epithelial versus mesenchymal Arhgef11 isoforms, we transfected cDNAs encoding FLAG-tagged proteins of each isoform to rescue *Arhgef11* KO cells. We noted that the epithelial ARHGEF11isoform (Epi Rescue) restored MLC phosphorylation, whereas the mesenchymal isoform (Mes Rescue) did so only partially (Figure 5D). These findings suggested that the epithelial isoform was able to more efficiently activate RhoA via GTP loading. We therefore used the RhoA activation assay with the Rho GTP-binding domain (RBD) of Rhotekin fused with glutathione S-transferase (GST) (Reid et al., 1996). We used lysates from Py2T cells transfected with cDNAs for the epithelial or mesenchymal ARHGEF11 isoforms in GST pulldowns of RhoGTP and immunoblotted for RhoA. These experiments demonstrated that the epithelial isoform was more effective in RhoA activation than the mesenchymal isoform (Figure 5E). Similarly, we noted that the epithelial isoform was able to partially restore barrier function in TEER and FITC dextran assays, whereas the mesenchymal isoform was less efficient (Figures 5F and 5G). While these experiments were carried out using cDNAs for the human ARHGEF11 isoforms, we observed the same preferential rescue of TEER and tracer flux using cDNAs encoding the corresponding mouse Arhgef11 isoforms (Figure S4).

Deletion of Arhgef11 Mesenchyme-Specific Exon 37 in *Esrp1;Esrp2* DKO Epithelial Cells Rescues TJ Function and MLC Phosphorylation by Abrogating an Interaction with Inhibitory Pak4

To test more directly whether the isoform switch in Arhgef11 contributed to the barrier defect in Esrp ablated epithelial cells, we used CRISPR/Cas9 to delete exon 37 in *Esrp1;Esrp2* DKO Py2T cells. We isolated 2 clones using 2 independent single guide RNA (sgRNA) pairs in which we confirmed exon 37 deletion by PCR and reversion of splicing toward the epithelial isoforms by RT-PCR (Figures 5H–5J). This switch in endogenous Arhgef11 splicing was able to partially restore barrier function *in vitro* to *Esrp1;Esrp2* DKO cells using TEER and FITC-dextran assays (Figures 5K and 5L). In addition, we determined that deletion of exon 37 partially restored MLC phosphorylation and RhoA activation to *Esrp* ablated cells (Figures 5M and 5O). Our results are consistent with the hypothesis that the epithelial isoform of Arhgef11 is more effective than the mesenchymal isoform in maintaining epithelial cell barriers due to increased MLC phosphorylation in response to RhoA activation, and they strongly suggest that this isoform switch in *Esrp* depleted or ablated cells contributes to the loss of MLC phosphorylation altered barrier function. A direct interaction of ARHGEF11 with ZO-1 was previously shown to be mediated by a C-terminal region of ARHGEF11 in a region where the Esrp-regulated alternative exon is located, suggesting that differential binding to ZO-1 may account for their differential activities. However, in immunoprecipitations from 293T cells transiently transfected with FLAG-tagged cDNAs of both isoforms, we observed that both isoforms bound ZO-1 at apparent similar levels of efficiency (Figure 6A). We also generated both 293T and Py2T cells stably expressing either the epithelial or mesenchymal isoform of ARHGEF11 and similarly noted that both interacted with ZO-1 in pulldown assays (Figure S5). We noted that

Author Manuscript Author Manuscript Author Manuscript Author Manuscript

the alternative exon was not located within or near any canonical domains in ARHGEF11, including the Rho binding Dbl homology (DH) domain (see Figure 3B). We therefore explored protein interaction databases and the literature to identify candidate protein-protein interactions with Arhgef11 that may be isoform specific in the regulation of its activity. Our literature search uncovered an interaction of p21-activated kinase 4 (PAK4) with ARHGEF11 that was detected by co-immunoprecipitation, as well as a yeast 2-hybrid screen for proteins interacting with the C-terminal domain of ARHGEF1, which had been shown to have GEF inhibitory functions (Barac et al., 2004; Huttlin et al., 2015). A C-terminal region of ARHGEF11 (amino acids 1081–1523 in the reference mesenchymal isoform) was confirmed to be sufficient for PAK4 binding in 293T cells (Barac et al., 2004). This study demonstrated that PAK4 binding resulted in serine and threonine phosphorylation of ARHGEF11 and inhibited RhoA activation. Because this C-terminal domain included the Esrp-regulated exon, we tested whether there was a difference in binding to PAK4 by the epithelial and mesenchymal isoforms that may also account for decreased RhoA activation by the mesenchymal isoform. We transfected 293T cells with cDNAs for FLAG-tagged human epithelial and mesenchymal ARHGEF11 isoforms followed by anti-FLAG immunoprecipitation. We noted that the mesenchymal but not the epithelial isoform was able to efficiently immunoprecipitate (IP) endogenous PAK4 (Figures 6B, 6C, and S6). We also showed that there was preferential association of the epithelial isoform with RhoA using an antibody that recognizes both activated and unactivated forms of RhoA (Figure 6C). Reverse co-IP of endogenous PAK4 followed by immunoblotting for FLAG-tagged ARHGEF11 in transfected cells confirmed the preferential association of PAK4 with the mesenchymal isoform (Figure 6C). We also demonstrated that ectopic expression of the epithelial ARHGEF11 isoform in these cells was associated with higher levels of activated RhoA (Figures 6D and S6). To confirm the isoform-specific interaction of Arhgef11 with Pak4 *in vivo*, we used the mammalian protein-protein interaction trap (MAPPIT) assay. In this assay, protein bait-prey interacting pairs are able complement a signal transducer and activator of transcription (STAT)-dependent reporter with a luciferase-based readout for positive protein-proteins interactions (Eyckerman et al., 2001). We used the previously established framework for scoring positive interactions by calculating the experimental-to-control ratio (ECR), as described previously and in Method Details (Venkatesan et al., 2009). Using this assay, we verified that PAK4 directly interacts with mesenchymal ARHGEF11 but not with epithelial ARHGEF11 *in vivo* (Figure 6E). These results indicate that PAK4 binding to the mesenchymal isoform of ARHGEF11 inhibits its ability to activate RhoA and induce MLC phosphorylation to maintain TJ integrity and function (Figure 6F).

DISCUSSION

In the past 10 years, technological advances have led to the identification of large-scale AS networks in different cell types and those that are controlled by specific splicing factors, including cell- or tissue-specific regulators. It has been shown that these networks regulate splicing in sets of genes that function in common or related pathways and processes that maintain important cellular phenotypes. The importance of cell type-specific splicing has been further demonstrated by the identification of pathologies that result when splicing factors, particularly those expressed in neurons and/or muscle such as Nova, Srrm4, Rbfox,

Author Manuscript Author Manuscript Author Manuscript Author Manuscript

and Mbnl, are ablated in mice (Gehman et al., 2011; Jensen et al., 2000; Kalsotra et al., 2008; Nakano et al., 2012). However, it remains a major challenge to determine which splicing changes observed in these tissues following splicing factor ablation give rise to these disease-related phenotypes. The functional characterization of different protein isoforms that result from AS holds promise both for identifying genes that are also associated with human disease and to further dissect molecular mechanisms that relate to the phenotypes observed when specific splicing factors are inactivated. The identification of isoform-specific protein-protein interactions and cellular assays related to specific phenotypes can be used to begin to interrogate gene functions at the exon level. While germline deletion of *Esrp1* with or without *Esrp2* was associated with defects in multiple organs and tissues, conditional deletion of *Esrp1* and *Esrp2* in the skin was associated with an epidermal barrier defect. In this study, we established that this phenotype is due at least in part to a disruption in the organization of TJs and in their ability to restrict the flow of ions and water across these cell-cell adhesion complexes. While germline ablation of *Esrp1* and *Esrp2* was associated with hypoplastic epidermis and lethality, the induction of gene ablation postnatally after the completion of embryonic skin development was not lethal, but it did lead to altered TJ morphology and inflammation. Similar chronic changes have been previously observed in other models of epidermal barrier defects (Yang et al., 2010).

The TEER and tracer flux assays provided a means to begin to interrogate Esrp regulated transcripts for their role in the maintenance of epithelial cell integrity. Previous studies identified Arhgef11 as an interacting partner with the TJ protein ZO-1 and noted that its depletion led to the disruption of TJs through abrogation of MLC phosphorylation. We therefore investigated whether this important role of Arhegf11 in epithelial cells was more robustly carried out by the epithelial isoform than the mesenchymal isoform that is induced by ablation of the Esrps. While both isoforms interacted with ZO-1, we determined that the mesenchymal but not the epithelial Arhgef11 isoform interacts with PAK4, which inhibits RhoA activation. Reduced RhoA activation observed in *Esrp* KO cells leads to a reduction in MLC phosphorylation, which reduces contraction of the PJAR and disrupts TJs. Consistent with this model, ectopic expression of the epithelial ARHGEF11 isoform was more efficiently able to restore TJ function in *Arhgef11* KO cells than the mesenchymal isoform, as assessed by TEER and tracer flux assays. While the mesenchymal isoform was also able to partly restore TEER and inhibit tracer flux, we suspect that this was in part due to higher levels of expression than the endogenous protein, which likely was able to overcome inhibition by PAK4 by a titration effect (Figures 5F and 5G). When we converted endogenous Arhgef11 splicing back to exclusive production of epithelial isoforms in *Esrp1;Esrp2* DKO cells, we observed a partial rescue of barrier function. However, this partial rescue also indicates that the altered splicing of Arhgef11 alone is not the only splicing change that accounts for the disruption of the TJs in the epidermis. Further assays of TJ function of other Esrp regulated targets will likely uncover additional genes that contribute to the maintenance of these important dynamic structures through the activity of epithelial-specific isoforms. Several of these targets, such as Nf2 and Arhgap17, have previously been shown to have important roles in the maintenance of epithelial barriers, and it is possible that these functions are preferentially carried out by epithelial isoforms (Gladden et al., 2010; Lee et al., 2016). We note that a recent study also described

Author Manuscript Author Manuscript Author Manuscript Author Manuscript

differential activities of the same isoforms of ARHGEF11, showing that the mesenchymal but not the epithelial isoform promoted cell migration and invasion in mesenchymal cells (Itoh et al., 2017). These findings are consistent with observations that TJs are disrupted during the EMT and our findings showing an important role for the epithelial ARHGEF11 isoform in TJ maintenance. We note, however, that this study presented a model wherein the epithelial but not the mesenchymal isoform interacted with ZO-1, in contrast to our findings. While we cannot definitively account for our different findings, we note that their study used cotransfection of cDNAs of ARHGEF11 cDNAs and a GFP fusion with a partial ZO-1 derived protein sequence. In our studies, we showed that both isoforms were able to co-IP endogenous ZO-1 (Figure 6A). Furthermore, we also showed that both isoforms were able to co-IP endogenous ZO-1 when stably expressed in both 293T cells and the mouse epithelial Py2T cell line (Figure S5).

Our study provides further evidence of the role AS plays in important cell functions via the regulation of differential protein-protein interactions and illustrates an example whereby the expression of an epithelial cell-specific protein isoform contributes to the important function of epithelial cell barriers. We also note that small GTPase effectors and regulators are among the enriched terms in Esrp-regulated genes as well as targets of other cell type-specific splicing factors. Previous studies have identified examples of other small GTPases and their regulators that have alternative isoforms with distinct and biologically important differential functions (Ellis et al., 2012; Hinman et al., 2014; Radisky et al., 2005; Singh et al., 2014). While our studies support previous work showing that Arhgef11 plays an important role in the maintenance of epithelial TJs, it bears mentioning that mice with germline KO of Arhgef11 were shown to be viable with phenotypes unrelated to epithelial barrier functions (Chang et al., 2015; Mikelis et al., 2013). While it is possible that subtle alterations in epithelial junctions may have been overlooked in these mice, we suspect that Arhgef11 ablation in early-stage embryos may lead to compensation by other Rho GTPase effectors. Consistent with this possibility, ablation of *Arhgef11* together with its paralog Arhgef12 resulted in embryonic lethality (Mikelis et al., 2013). There are also several other Rho GTPase effectors such as Arhgef2 and Arhgef18 that have been linked to the regulation of TJ-based barriers that may also be co-opted to maintain epithelial barriers in response to germline loss of *Arhgef11* functions (Itoh et al., 2014; Zihni et al., 2016). Consistent with the possibility that conditional deletion of *Arhgef11* at a later developmental stage may be associated with more severe phenotypes, another group showed that depletion of *Arhgef11* using siRNAs in neuroepithelial cells of chick embryos was associated with the loss of MLC phosphorylation and the failure of neural tube formation (Nishimura et al., 2012). Genetic compensation in response to germline KO of otherwise essential genes is a widespread phenomenon, and thus we suspect that conditional ablation of *Arhgef11* in the epidermis may validate the function of Arhgef11 in barrier function *in vivo* (El-Brolosy and Stainier, 2017). In any event, our studies have identified a context in which we observe a clear isoform-specific difference of a protein involved in the regulation of TJs and provided a mechanism to account for these differences.

Our studies have identified Arhgef11 as an Esrp regulated gene that contributes to epithelial barrier function in the skin through the regulation of TJ integrity. However, further studies are needed to identify additional examples of epithelial cell type-specific protein isoforms

Author Manuscript Author Manuscript Author Manuscript Author Manuscript

that contribute to the barrier functions in these cells, as well as those in other epithelial cell layers such as the gastrointestinal system and the lung. In addition to uncovering further examples of genes with isoform-specific functions in epithelia, such investigations will begin to unravel the molecular mechanisms and protein interaction networks that are specifically relevant to the general maintenance of epithelial cell properties. There are also a host of other disease-relevant phenotypes in both *Esrp1* KO and *Esrp1;Esrp2* DKO mice that are likely due to the loss of a number of other epithelial specific isoforms that are regulated by the Esrps (Bebee et al., 2015,2016; Rohacek et al., 2017). It will be challenging to find *in vitro* and *in vivo* assays that can identify important AS events whose misregulation leads to these phenotypes. With the advances in CRISPR/Cas9 and related genome-editing technologies, it is now possible to begin the systematic generation of mice that only express 1 of 2 different splice variants to further extend our understanding of AS in a broad set of different cell types.

In conclusion, we have identified Arhgef11 as one of the Esrp1 splicing targets that underlies barrier defects in the epidermis, which result from the disruption of TJs. In addition to providing a detailed mechanistic dissection of the differences in Arhgef11 isoforms, these findings provide a further example whereby alterations in protein-protein interactions due to AS can have profound functional consequences at the level of essential cellular functions.

STAR★METHODS

CONTACT FOR REAGENT AND RESOURCE SHARING

Further information and requests for resources and reagents should be directed to and will be fulfilled by the Lead Contact, Russ P. Carstens (russcars@upenn.edu). Where indicated the requests will be fulfilled with simple Material Transfer Agreement (MTA).

EXPERIMENTAL MODEL AND SUBJECT DETAILS

Mice—Generation of Esrp1 KO *(Esrp1*$^{-/-}$*;Esrp2*$^{+/+}$), Esrp DKO (*Esrp1*$^{-/-}$*;Esrp2*$^{-/-}$), and mice with floxed Esrp1 alleles (*Esrp1*$^{f/f}$ and *Esrp1*$^{f/f}$*;Esrp2*$^{-/-}$) for conditional gene ablation were described previously (Bebee et al., 2015). Briefly, exons 7 to 9 were floxed and mice with germline Esrp1 KO were derived in crosses with Zp3-Cre transgenic females. Esrp2 KO alleles include a LacZ reporter in place of the entire Esrp2 coding sequences. To test postnatal Esrp function in epidermis, *Esrp1*$^{f/f}$*;Esrp2*$^{-/-}$*; K5-rtTA; tetO-Cre* mice were generated. Transgenic *Keratin-5 rtTA* (K5-rtTA) (Mucenski et al., 2003) mice, which express Cre under the Keratin 5 promoter in basal epidermal cells and epithelial cells of the hair follicle were obtained from Sarah Millar (University of Pennsylvania) and *tetO-Cre* strains (Diamond et al., 2000) were obtained from JAX. Mice carrying the *K5-rtTA* promotor were bred with mice carrying the *tetO-Cre* transgene and with mice carrying a loxP-flanked Esrp1 allele. Esrp1 deletion in epidermis was induced by Doxycycline (Bio-Serv) feeding after birth. Both male and female mice were included in the study and there were no apparent differences in the observed phenotypes between male and female mice. All experiments involving mice were approved by the University of Pennsylvania Institutional Animal Care and Use Committee (IACUC).

Author Manuscript Author Manuscript Author Manuscript Author Manuscript

Cell lines—293T cells and Py2T were grown in DMEM with 10% FBS at 37°C and 5% CO_2. Py2T cell are derived from a breast tumor of an MMTV-PyMT transgenic mouse. Mouse MCK-6 keratinocyte cells were maintained under low calcium and low serum (2% FBS) defined-KSFM media in collagen type-1 coated dishes.

METHOD DETAILS

Plasmids for transfections of cDNAs—pIBX and pIPX expression vectors, that contain IRES driven blasticidin and puromycin selection markers, respectively were previously described (Warzecha et al., 2009). To construct Arhgef11 (mouse) and ARHGEF11 (human) expression vector, initially Mouse Arhgef11 and human ARHGEF11 cDNA for mesenchymal isoforms were commercially purchased (see Key Resources Table). The PCR amplified coding sequence for Mes-Arhgef11 and Mes-ARHGEF11 was inserted into EcoRI and NotI digested vector. The cDNAs for the epithelial isoforms (Epi-Arhgef11 and Epi-ARHGEF11) were obtained by RT-PCR of the region where the exon is skipped from epithelial cells that were then inserted in NheI and NotI or BglII and NotI digested pIBX or pIPX ARHGEF11 or Arhgef11 expression vectors, respectively to replace the same regions that contained the mesenchymal exon. *Arhgef11* KO Py2T cells were transiently transfected with pIBX based vectors using Lipofectamine 3000 and selected in 10 ug/ml blasticidin for 48 hours prior to assays. Transient transfections of pIPX based versions of ARHGEF11 isoforms in 293T cells (Figure 6) were carried out using Mirus 293T along with pIPX empty vector control and harvested after 48 hours. Stable transfections of 293T and Py2T with pIPX based ARHGEF11 cDNAs were carried out using Mirus 293T and Lipofectamine 3000, respectively and selected in puromycin for over 3 weeks. The pSg-Puro plasmid was created for transfection of sgRNAs with a vector containing a puromycin selection cassette. It was generated by removal of the Cas9 coding sequence from px300 with AgeI and EcoRI and replacing it with a coding sequence for a puromycin selection cassette. Lentiviral production and transduction were performed as previously described (Warzecha et al., 2010; Yang et al., 2016b).

Plasmids for Lentiviral transduction of shRNAs—Vectors for KD of Esrp1 and Esrp2 were constructed by digesting pLKO.1-puro with AgeI and EcoR1 and cloning in annealed oligo pairs in Table S3. After 20 hours incubation, the media was replaced with fresh DMEM with 10% FBS, and virus was harvested after an additional 24 hours. Target cells were transduced with a 50/50 mixture of viral supernatant and DMEM with 10% FBS. Cells were drug selected using 2 μg/ml puromycin for 96 to 120 hours. RNA or protein was harvested 7 to 8 days after viral infection.

CRISPR/Cas9-mediated KO

-Cas9 stable cell Generation: To generate py2T cells with KO of Esrp1, Esrp2, and Arhgef11 we purchased the PX330 vector from Addgene (#42230). PX330 was digested with AgeI and EcoRI to obtain the coding sequences for human codon-optimized SpCas9 (hSpCsn1). This fragment was inserted into the pIBX vector and we named it pIBX-Cas9. We transfected the pIBX-Cas9 vector into Py2T cells using Lipofectamine 3000 according the manufacturers' protocols. 48 hours post-transfection, the cells were selected using 10ug/ml Blasticidin. A population of Py2T cells that stably express Cas9 was obtained by

Author Manuscript Author Manuscript Author Manuscript Author Manuscript

maintaining Blasticidin selection for 20 days. Single cell clones were obtained by serial dilution. Protein lysates from several clones were harvested in RIPA buffer and the expression of Cas9 protein was confirmed by Western.

-Esrp1 KO: Py2T cells were transiently transfected Lipofectamine 3000 in 24well plate. Cells were transfected with a total of 1mg of total DNA: 250ng of pX335 with guide 8A, 250ng of pX335 with guide 16A, 250ng pIPX-mCherry. After 24hrs, transfected cells were enriched by the addition of medium containing puromycin at 5 μg/mL for 72hrs. Cells were allowed to recover for overnight in medium with selection antibiotic. Clonal cells were isolated in 96-well plate format. Genomic DNA was amplified from clonal lines using primers flanking the nickase targeted site. The PCR products were cloned in a blunt vector, and after transformation colonies were submitted for sequencing to identify indels or the knock-in of the FLAG tag at the Esrp1 locus, to generate a FLAG Esrp1 fusion.

-Esrp 1/2 DKO: *Esrp1* KO Py2T cells were transiently transfected with 400ng pX330 without guide sequence (for expression of Cas9) and 300ng with pSg-Puro vectors containing guide sequences targeting introns 1 and 3 for removal of exons 2 and 3. Cells were transfected using Lipofectamine 3000 in 24well plates. After 24hrs, transfected cells were selected by the addition of medium containing puromycin at 10 ng/mL for 72hrs. Cells were allowed to recover overnight in medium without selection. Clonal cells were isolated in 96-well format. Genomic DNA was amplified from clonal lines using primers flanking the targeted exon. The PCR products were confirmed by sequencing.

-Arhgef11 KO: We obtained pSg-Puro vectors with guide RNAs targeting the introns flanking *Arhgef11* exon 2 (which is the first non-multiple of three constitutive exon). Upon transfection of a pair of sgRNA plasmids in the Py2T Cas9 clone we isolated clones following puromycin selection where Arhgef11 exon 2 was deleted. The KO of Arhgef11 was then confirmed by PCR and Westernblot. For deletion of Arhgef11 exon 37 we designed two pairs of sgRNAs in the introns flanking this exon and isolated clones in which exon 37 deletion was confirmed for each pair of sgRNAs.

Isolation of RNA, Reverse Transcription, and RT-PCR—RNA for RT-PCR experiment was isolated from PY2T and MKC-6 cells via TriZol (Invitrogen) and Zymo-Spin IIC columns (Zymo Research). RNA isolation of E18.5 embryo epidermis was described previously (Bebee et al., 2015). Reverse transcription and RT-PCR was performed as described previously (Bebee et al., 2015; Warzecha et al., 2009).

Immunofluorescence—Frozen sections of the mice epidermis were fixed for 10 minutes in acetone at −20°C. Paraffin section deparaffinized in xylene and rehydrated using graded ethanol. Cultured cells were fixed in cold methanol 5 minutes and then in acetone 15 s at 4°C. Antigen retrieval was performed using unmasking solution (Vector Laboratories) or 0.5% Triton X-100 in humidified chamber. Samples were blocked with 0.5%nonfat dry milk and 10% horse serum in PBST 1hour at RT. Primary antibodies were incubated overnight at 4°C. After washing three times with PBST, Alexa 488 or Alexa 594labeled secondary antibodies (Invitrogen) were applied for 30 minutes at RT, followed by another wash and

Author Manuscript Author Manuscript Author Manuscript Author Manuscript

mounted with Prolong Gold antifade reagent with DAPI (Invitrogen).Images were taken using an Olympus BX43.

Immunoblot—Total cell lysates were harvested in RIPA buffer and immunoblotting was performed as described previously (Bebee et al., 2015).Briefly, Total proteins were separated by SDS-PAGE and then transferred to nitrocellulose membranes. After blocking for 1 hour with 5% Non-fat dry milk powder or 5% bovine serum albumin (BSA) in Tris buffered saline-tween 20 (TBST), membranes were incubated overnight at 4°C with the primary antibodies. Subsequently, membranes were washed in TBST and incubated for 1 hour with the appropriate secondary antibodies. After washing thrice for 10 minutes with TBST, proteins were visualized by chemiluminescent detection (Thermo Scientific).

Co-IP—Total cell lysates were prepared as described in NP-40 buffer (1% NP-40, 150mM NaCl, 2mM EDTA, 50mM Tris-HCl, pH8.0). For the FLAG IP, proteins were incubated with anti-FLAG affinity gel (Sigma) for 1hour at 4°C with rotating. Beads were washed 4 times with wash buffer, and then resuspended in protein loading buffer. For the PAK4 IP, lysates were pre-cleared with Protein A Agarose (Invitrogen) for 1 hour at 4°C and then incubated with 10 μg of anti-PAK4 antibody (Cell Signaling), overnight at 4°C. Antigen-Antibody bound Protein A Agarose pellets were washed 4 times with wash buffer, and then resuspended in protein loading buffer. The released proteins were fractionated by Bis-Tris 4%–20% SDS-PAGE (Invitrogen), and then transferred to nitrocellulose membranes. Immunoblotting was performed as described above using antibodies RhoA, PAK4, Flag, or β-actin antibody as described above.

Rho Activation assay—All the materials were from the Rho Activation Assay Biochem Kit (Cytoskeleton, Cat#BK036) and we followed the methods using the manufacturers' protocols. Briefly, Cell lysates were harvested in lysis buffer. Proteins incubated with 50μg of Rhotekin-RBD beads at 4°C on rotator for 1hour. Beads were subsequently washed with wash buffer. Pull-down and immunoblotting step are described above.

Transepithelial electrical resistance (TEER) assay and FITC-dextran flux assay —MKC-6 Keratinocytes or Py2T epithelial cells were grown on polycarbonate Transwell filters (Corning) in low glucose and calcium free media. After fully confluent, a calcium shift was begun with addition of media containing 1.5Mm $CaCl_2$. Before measurement, electrodes were equilibrated and sterilized with 70% ethanol and PBS. TEER was measured with a Millicell® ERS-2 Voltohmmeter (Millipore). To obtain the monolayer resistance, the empty transwell (blank) value was subtracted from the each resistance of the samples. Values were expressed in $\Omega * cm^2$and measurement was performed every 24hours after calcium switch at indicated times. Mean results are calculated from three independent experiment. After final TEER measurement, each upper chamber was washed with PBS and moved to new 12 wells plate for the following FITC-dextran flux assay. 0.5mg/ml FITC-dextran (4kDa) (Sigma-Aldrich) was applied to the cell monolayers and plates were incubated for 120-150mins at 37°C. After incubation, the PBS containing penetrated FITC-dextran from the transwells was collected and fluorescence intensity was measured using a

Author Manuscript Author Manuscript Author Manuscript Author Manuscript

Typhoon FLA 9500. The amount of FITC-dextran was quantified and calculated using a ImageQuant TL, version 7.0

Biotin injection assay—To test the TJ barrier permeability in mice, 10 mg/ml EZ-Link sulfo-NHS-LC-biotin (Pierce Chemical) in PBS containing 1 mM $CaCl_2$was intradermally injected underneath the dermis of the E18.5 mice back skin. After 30 minutes of incubation at 37°C, mice back skin was isolated, embedded in Tissue-Tek, and frozen. 4% Paraformaldehyde fixed section was immunostained with TJ marker, anti-Occludin antibody. After washing step, Alexa 594labeled secondary antibodies (Life technologies)for TJ marker and Alexa 488 Streptavidin (Life technologies)for biotin labeling were applied for 30 minutes at RT. Followed by another washing and mounted with Prolong Gold antifade reagent with DAPI (Invitrogen).Image were taken using an Olympus BX43.

MAPPIT assay—The plasmids pMG1-SVT, pSEL+2L-hMal, pMG1-GW, pSEL+2L-GW and pXP2d2-rPAP1-luci were obtained from Jan Tavernier. The cDNA for ARHGEF11 Mesenchymal and Epithelial isoforms were obtained as previously described, and were subcloned in pMG1 (prey) and pSEL+2L (bait) using EcoRI/NotI and XhoI/NotI respectively. The cDNA for PAK4 (HsCD00376906) was obtained from the PlasmID Repository at Harvard Medical School. PAK4 was cloned using Gateway Recombination LR Cloning (Thermo Fisher Scientific) into the pMG1-GW (prey) and pSEL+2L-GW (bait). All plasmids were verified by Sanger Sequencing. The SV40 large T-antigen was obtained from Addgene (#1780) and following PCR amplification of amino acids 261-708, was cloned into bait and prey vectors using Gateway recombination. MAPPIT transfections and assay were performed as previously described (Venkatesan et al., 2009). Briefly, HEK293T cells were seeded in 96-well plate at a density of 12000 cells/well. Prior to plating wells were treated with 20mg/mL collagen to aid adherence of HEK293T. Cells were transfected 24hrs after seeding with 45ng of bait containing vector, 45ng of prey containing vector and 10ng of luciferase reporter plasmid, in two sets of triplicates, using TransIT-293 (Mirus). On the following day, cells were stimulated with 5ng/mL human Erythropoietin (Cell Signaling Technology, 6980SC) in triplicate. Luciferase readings were collected 24hrs after hEpo stimulation, by lysing the cells Britelite Plus (Perkin Elmer) and measurements were recorded using DTX Multimode plate reader. Interactions of ARHGEF11 Mesenchymal and Epithelial and PAK4 were tested with each cDNA cloned in prey and bait plasmid. Positive protein protein-protein interactions were identified as previously described (Venkatesan et al., 2009), by identifying Experiment to Control Ratio (ECR) > 10 in any orientation. ECR for the MAPPIT was calculated as the fold-induction value with bait and prey, divided by the fold-induction value with bait and irrelevant prey, or prey and irrelevant bait. The irrelevant interacting protein tested was SV40 large T-antigen. Fold induction was calculated as the ratio of luciferase reading of bait:prey interaction in the presence of hEpo with luciferase reading of bait:prey interaction in the absence of hEpo.

QUANTIFICATION AND STATISTICAL ANALYSIS

Statistical analyses of the data were performed in Graphpad Prism. Error bars represent ± SD of experiments performed in at least one biological triplicate. Statistical significance was calculated by t test and denoted as follows: * = $p < 0.01$, $p < 0.005$; **, $p < 0.001$; ***, p <

Author Manuscript Author Manuscript Author Manuscript Author Manuscript

0.0001; ****. Results of statistical analysis are presented in Figure Legends 1, 4, and 5 where the value for n in each case is provided.

Supplementary Material

Refer to Web version on PubMed Central for supplementary material.

ACKNOWLEDGMENTS

The Skin Biology and Diseases Resource-based Center (SBDRC) at the University of Pennsylvania assisted in consultation and tissue processing. We thank Dr. Stephen Prouty for technical expertise in skin and tissue histology, Dr. Sarah Millar's lab for mouse and technical and experimental guidance, and Dr. John Seykora for phenotype analysis and consultation. This work was funded by NIH grants RO1AR066741, R56AR066741, and P30AR057217 (to R.P.C.).

REFERENCES

Augustin I, Gross J, Baumann D, Korn C, Kerr G, Grigoryan T, Mauch C, Birchmeier W, and Boutros M (2013). Loss of epidermal Evi/Wls results in a phenotype resembling psoriasiform dermatitis. J. Exp. Med 210, 1761–1777. [PubMed: 23918954]

Barac A, Basile J, Vázquez-Prado J, Gao Y, Zheng Y, and Gutkind JS (2004). Direct interaction of p21-activated kinase 4 with PDZ-RhoGEF, a G protein-linked Rho guanine exchange factor. J. Biol. Chem 279, 6182–6189. [PubMed: 14625312]

Bebee TW, Park JW, Sheridan KI, Warzecha CC, Cieply BW, Rohacek AM, Xing Y, and Carstens RP (2015). The splicing regulators Esrp1 and Esrp2 direct an epithelial splicing program essential for mammalian development. eLife 4, e08954.

Bebee TW, Sims-Lucas S, Park JW, Bushnell D, Cieply B, Xing Y, Bates CM, and Carstens RP (2016). Ablation of the epithelial-specific splicing factor Esrp1 results in ureteric branching defects and reduced nephron number. Dev. Dyn 245, 991–1000. [PubMed: 27404344]

Blencowe BJ (2017). The relationship between alternative splicing and proteomic complexity. Trends Biochem. Sci 42, 407–408. [PubMed: 28483376]

Buljan M, Chalancon G, Eustermann S, Wagner GP, Fuxreiter M, Bateman A, and Babu MM (2012). Tissue-specific splicing of disordered segments that embed binding motifs rewires protein interaction networks. Mol. Cell 46, 871–883. [PubMed: 22749400]

Chang YJ, Pownall S, Jensen TE, Mouaaz S, Foltz W, Zhou L, Liadis N, Woo M, Hao Z, Dutt P, et al. (2015). The Rho-guanine nucleotide exchange factor PDZ-RhoGEF governs susceptibility to diet-induced obesity and type 2 diabetes. eLife 4, e06011. [PubMed: 26512886]

Chen M, and Manley JL (2009). Mechanisms of alternative splicing regulation: insights from molecular and genomics approaches. Nat. Rev. Mol. Cell Biol. 10, 741–754. [PubMed: 19773805]

Cieply B, and Carstens RP (2015). Functional roles of alternative splicing factors in human disease. Wiley Interdiscip. Rev. RNA 6, 311–326. [PubMed: 25630614]

De Benedetto A, Rafaels NM, McGirt LY, Ivanov AI, Georas SN, Cheadle C, Berger AE, Zhang K, Vidyasagar S, Yoshida T, et al. (2011). Tight junction defects in patients with atopic dermatitis. J. Allergy Clin. Immunol 127, 773–786.e1–7. [PubMed: 21163515]

Diamond I, Owolabi T, Marco M, Lam C, and Glick A (2000). Conditional gene expression in the epidermis of transgenic mice using the tetracycline-regulated transactivators tTA and rTA linked to the keratin 5 promoter. J. Invest. Dermatol 115, 788–794. [PubMed: 11069615]

Dittmar KA, Jiang P, Park JW, Amirikian K, Wan J, Shen S, Xing Y, and Carstens RP (2012). Genome-wide determination of a broad ESRP-regulated posttranscriptional network by high-throughput sequencing. Mol. Cell. Biol 32, 1468–1482. [PubMed: 22354987]

El-Brolosy MA, and Stainier DYR (2017). Genetic compensation: a phenomenon in search of mechanisms. PLoS Genet. 13, e1006780. [PubMed: 28704371]

Author Manuscript Author Manuscript Author Manuscript Author Manuscript

Ellis JD, Barrios-Rodiles M, Colak R, Irimia M, Kim T, Calarco JA, Wang X, Pan Q, O'Hanlon D, Kim PM, et al. (2012). Tissue-specific alternative splicing remodels protein-protein interaction networks. Mol. Cell 46, 884–892. [PubMed: 22749401]

Eyckerman S, Verhee A, der Heyden JV, Lemmens I, Ostade XV, Vandekerckhove J, and Tavernier J (2001). Design and application of a cytokine-receptor-based interaction trap. Nat. Cell Biol 3, 1114–1119. [PubMed: 11781573]

Furuse M, Hata M, Furuse K, Yoshida Y, Haratake A, Sugitani Y, Noda T, Kubo A, and Tsukita S (2002). Claudin-based tight junctions are crucial for the mammalian epidermal barrier: a lesson from claudin-1-deficient mice. J. Cell Biol 156, 1099–1111. [PubMed: 11889141]

Gehman LT, Stoilov P, Maguire J, Damianov A, Lin CH, Shiue L, Ares M, Jr., Mody I, and Black DL (2011). The splicing regulator Rbfox1 (A2BP1) controls neuronal excitation in the mammalian brain. Nat. Genet 43, 706–711. [PubMed: 21623373]

Gladden AB, Hebert AM, Schneeberger EE, and McClatchey AI (2010). The NF2 tumor suppressor, Merlin, regulates epidermal development through the establishment of a junctional polarity complex. Dev. Cell 19, 727–739. [PubMed: 21074722]

Hinman MN, Sharma A, Luo G, and Lou H (2014). Neurofibromatosis type 1 alternative splicing is a key regulator of Ras signaling in neurons. Mol. Cell. Biol 34, 2188–2197. [PubMed: 24710274]

Huttlin EL, Ting L, Bruckner RJ, Gebreab F, Gygi MP, Szpyt J, Tam S, Zarraga G, Colby G, Baltier K, et al. (2015). The BioPlex network: a systematic exploration of the human interactome. Cell 162, 425–440. [PubMed: 26186194]

Itoh M (2013). ARHGEF11, a regulator of junction-associated actomyosin in epithelial cells. Tissue Barriers 1, e24221. [PubMed: 24665387]

Itoh M, Tsukita S, Yamazaki Y, and Sugimoto H (2012). Rho GTP exchange factor ARHGEF11 regulates the integrity of epithelial junctions by connecting ZO-1 and RhoA-myosin II signaling. Proc. Natl. Acad. Sci. USA 109, 9905–9910. [PubMed: 22665792]

Itoh K, Ossipova O, and Sokol SY (2014). GEF-H1 functions in apical constriction and cell intercalations and is essential for vertebrate neural tube closure. J. Cell Sci 127, 2542–2553. [PubMed: 24681784]

Itoh M, Radisky DC, Hashiguchi M, and Sugimoto H (2017). The exon 38-containing ARHGEF11 splice isoform is differentially expressed and is required for migration and growth in invasive breast cancer cells. Oncotarget 8, 92157–92170. [PubMed: 29190905]

Ivanov AI (2008). Actin motors that drive formation and disassembly of epithelial apical junctions. Front. Biosci 13, 6662–6681. [PubMed: 18508686]

Jensen KB, Dredge BK, Stefani G, Zhong R, Buckanovich RJ, Okano HJ, Yang YY, and Darnell RB (2000). Nova-1 regulates neuron-specific alternative splicing and is essential for neuronal viability. Neuron 25, 359–371. [PubMed: 10719891]

Kalsotra A, Xiao X, Ward AJ, Castle JC, Johnson JM, Burge CB, and Cooper TA (2008). A postnatal switch of CELF and MBNL proteins reprograms alternative splicing in the developing heart. Proc. Natl. Acad. Sci. USA 105, 20333–20338. [PubMed: 19075228]

Kirschner N, and Brandner JM (2012). Barriers and more: functions of tight junction proteins in the skin. Ann. N Y Acad. Sci 1257, 158–166. [PubMed: 22671602]

Kubo A, Nagao K, and Amagai M (2012). Epidermal barrier dysfunction and cutaneous sensitization in atopic diseases. J. Clin. Invest 122, 440–447. [PubMed: 22293182]

Lee SY, Kim H, Kim K, Lee H, Lee S, and Lee D (2016). Arhgap17, a RhoGTPase activating protein, regulates mucosal and epithelial barrier function in the mouse colon. Sci. Rep 6, 26923. [PubMed: 27229483]

Mikelis CM, Palmby TR, Simaan M, Li W, Szabo R, Lyons R, Martin D, Yagi H, Fukuhara S, Chikumi H, et al. (2013). PDZ-RhoGEF and LARG are essential for embryonic development and provide a link between thrombin and LPA receptors and Rho activation. J. Biol. Chem 288, 12232–12243. [PubMed: 23467409]

Mucenski ML, Wert SE, Nation JM, Loudy DE, Huelsken J, Birchmeier W, Morrisey EE, and Whitsett JA (2003). beta-Catenin is required for specification of proximal/distal cell fate during lung morphogenesis. J. Biol. Chem 278, 40231–0238. [PubMed: 12885771]

Author Manuscript Author Manuscript Author Manuscript Author Manuscript

Nakano Y, Jahan I, Bonde G, Sun X, Hildebrand MS, Engelhardt JF, Smith RJ, Cornell RA, Fritzsch B, and Bánfi B (2012). A mutation in the Srrm4 gene causes alternative splicing defects and deafness in the Bronx waltzer mouse. PLoS Genet. 8, e1002966. [PubMed: 23055939]

Nishimura T, Honda H, and Takeichi M (2012). Planar cell polarity links axes of spatial dynamics in neural-tube closure. Cell 149, 1084–1097. [PubMed: 22632972]

Nusrat A, Giry M, Turner JR, Colgan SP, Parkos CA, Carnes D, Lemichez E, Boquet P, and Madara JL (1995). Rho protein regulates tight junctions and perijunctional actin organization in polarized epithelia. Proc. Natl. Acad. Sci. USA 92, 10629–10633. [PubMed: 7479854]

Pan Q, Shai O, Lee LJ, Frey BJ, and Blencowe BJ (2008). Deep surveying of alternative splicing complexity in the human transcriptome by high-throughput sequencing. Nat. Genet 40, 1413–1415. [PubMed: 18978789]

Pasparakis M, Haase I, and Nestle FO (2014). Mechanisms regulating skin immunity and inflammation. Nat. Rev. Immunol 14, 289–301. [PubMed: 24722477]

Radisky DC, Levy DD, Littlepage LE, Liu H, Nelson CM, Fata JE, Leake D, Godden EL, Albertson DG, Nieto MA, et al. (2005). Rac1b and reactive oxygen species mediate MMP-3-induced EMT and genomic instability. Nature 436, 123–127. [PubMed: 16001073]

Reid T, Furuyashiki T, Ishizaki T, Watanabe G, Watanabe N, Fujisawa K, Morii N, Madaule P, and Narumiya S (1996). Rhotekin, a new putative target for Rho bearing homology to a serine/threonine kinase, PKN, and rhophilin in the rho-binding domain. J. Biol. Chem 271, 13556–13560. [PubMed: 8662891]

Rohacek AM, Bebee TW, Tilton RK, Radens CM, McDermott-Roe C, Peart N, Kaur M, Zaykaner M, Cieply B, Musunuru K, et al. (2017). ESRP1 mutations cause hearing loss due to defects in alternative splicing that disrupt cochlear development. Dev. Cell 43, 318–331.e5. [PubMed: 29107558]

Schmitz A, Lazi'ć E, Koumaki D, Kuonen F, Verykiou S, and Rübsam M (2015). Assessing the in vivo epidermal barrier in mice: dye penetration assays. J. Invest. Dermatol 135, 1–4.

Sevilla LM, Latorre V, Sanchis A, and Pérez P (2013). Epidermal inactivation of the glucocorticoid receptor triggers skin barrier defects and cutaneous inflammation. J. Invest. Dermatol 133, 361–370. [PubMed: 22951731]

Shapiro IM, Cheng AW, Flytzanis NC, Balsamo M, Condeelis JS, Oktay MH, Burge CB, and Gertler FB (2011). An EMT-driven alternative splicing program occurs in human breast cancer and modulates cellular phenotype. PLoS Genet. 7, e1002218. [PubMed: 21876675]

Shkreta L, and Chabot B (2015). The RNA splicing response to DNA damage. Biomolecules 5, 2935–2977. [PubMed: 26529031]

Singh RK, Xia Z, Bland CS, Kalsotra A, Scavuzzo MA, Curk T, Ule J, Li W, and Cooper TA (2014). Rbfox2-coordinated alternative splicing of Mef2d and Rock2 controls myoblast fusion during myogenesis. Mol. Cell 55, 592–603. [PubMed: 25087874]

Troy TC, and Turksen K (1999). In vitro characteristics of early epidermal progenitors isolated from keratin 14 (K14)-deficient mice: insights into the role of keratin 17 in mouse keratinocytes. J. Cell. Physiol 180, 409–421. [PubMed: 10430181]

Tunggal JA, Helfrich I, Schmitz A, Schwarz H, Günzel D, Fromm M, Kemler R, Krieg T, and Niessen CM (2005). E-cadherin is essential for in vivo epidermal barrier function by regulating tight junctions. EMBO J. 24, 1146–1156. [PubMed: 15775979]

Turner JR (2000). 'Putting the squeeze' on the tight junction: understanding cytoskeletal regulation. Semin. Cell Dev. Biol 11, 301–308. [PubMed: 10966864]

Venkatesan K, Rual JF, Vazquez A, Stelzl U, Lemmens I, Hirozane-Kishikawa T, Hao T, Zenkner M, Xin X, Goh KI, et al. (2009). An empirical framework for binary interactome mapping. Nat. Methods 6, 83–90. [PubMed: 19060904]

Waldmeier L, Meyer-Schaller N, Diepenbruck M, and Christofori G (2012). Py2T murine breast cancer cells, a versatile model of TGFβ-induced EMT in vitro and in vivo. PLoS One 7, e48651. [PubMed: 23144919]

Wang ET, Sandberg R, Luo S, Khrebtukova I, Zhang L, Mayr C, Kingsmore SF, Schroth GP, and Burge CB (2008). Alternative isoform regulation in human tissue transcriptomes. Nature 456, 470–476. [PubMed: 18978772]

Author Manuscript Author Manuscript Author Manuscript Author Manuscript

Warzecha CC, Sato TK, Nabet B, Hogenesch JB, and Carstens RP (2009). ESRP1 and ESRP2 are epithelial cell-type-specific regulators of FGFR2 splicing. Mol. Cell 33, 591–601. [PubMed: 19285943]

Warzecha CC, Jiang P, Amirikian K, Dittmar KA, Lu H, Shen S, Guo W, Xing Y, and Carstens RP (2010). An ESRP-regulated splicing programme is abrogated during the epithelial-mesenchymal transition. EMBO J. 29, 3286–3300. [PubMed: 20711167]

Yang J, Meyer M, Müller AK, Böhm F, Grose R, Dauwalder T, Verrey F, Kopf M, Partanen J, Bloch W, et al. (2010). Fibroblast growth factor receptors 1 and 2 in keratinocytes control the epidermal barrier and cutaneous homeostasis. J. Cell Biol 188, 935–952. [PubMed: 20308431]

Yang X, Coulombe-Huntington J, Kang S, Sheynkman GM, Hao T, Richardson A, Sun S, Yang F, Shen YA, Murray RR, et al. (2016a). Widespread expansion of protein interaction capabilities by alternative splicing. Cell 164, 805–817. [PubMed: 26871637]

Yang Y, Park JW, Bebee TW, Warzecha CC, Guo Y, Shang X, Xing Y, and Carstens RP (2016b). Determination of a comprehensive alternative splicing regulatory network and combinatorial regulation by key factors during the epithelial-to-mesenchymal transition. Mol. Cell. Biol 36, 1704–1719. [PubMed: 27044866]

Yuki T, Haratake A, Koishikawa H, Morita K, Miyachi Y, and Inoue S (2007). Tight junction proteins in keratinocytes: localization and contribution to barrier function. Exp. Dermatol 16, 324–330. [PubMed: 17359339]

Zihni C, Mills C, Matter K, and Balda MS (2016). Tight junctions: from simple barriers to multifunctional molecular gates. Nat. Rev. Mol. Cell Biol 17, 564–580. [PubMed: 27353478]

Author Manuscript Author Manuscript Author Manuscript Author Manuscript

Highlights

- Ablation of *Esrp1* and *Esrp2* in mouse epidermis leads to tight junction defects
- A switch in splicing of exon 37 in Arhgef11 transcripts produces isoforms that bind Pak4
- Inhibition of Arhgef11 by Pak4 causes a reduction in RhoA activation at tight junctions
- Restoration of epithelial Arhgef11 isoforms partially rescues tight junction defects

Author Manuscript Author Manuscript Author Manuscript Author Manuscript

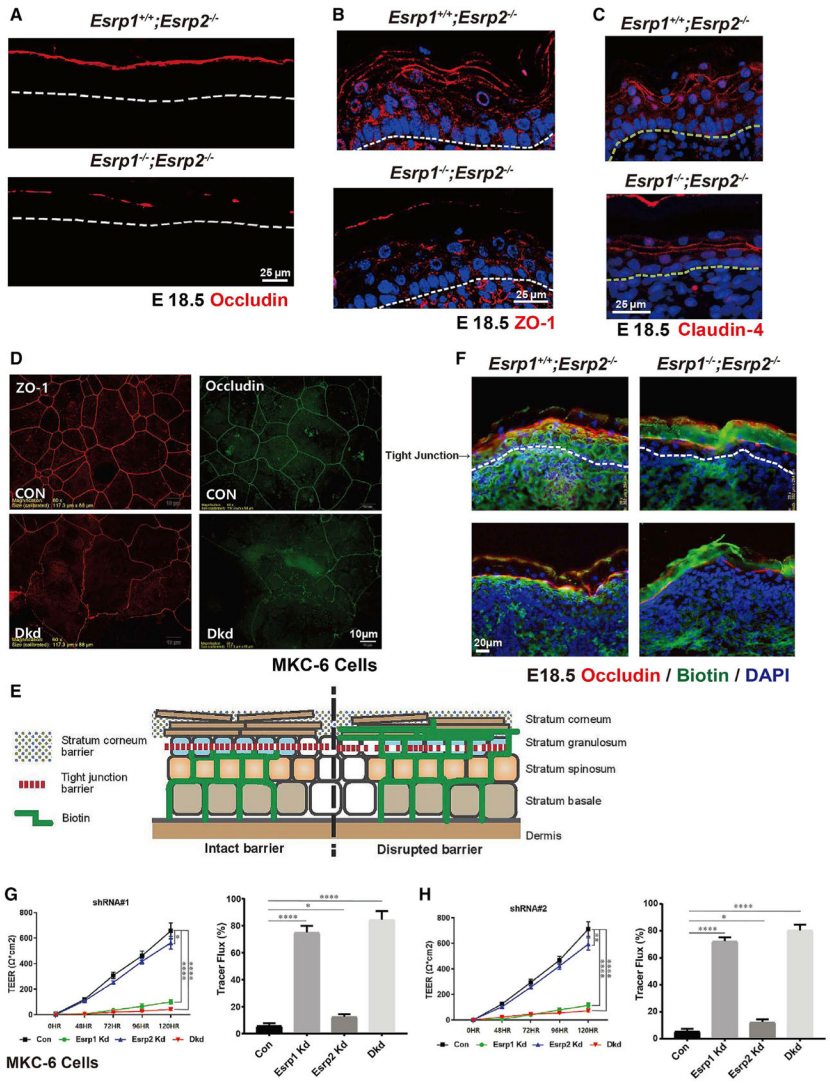

Figure 1. Esrp Ablation in Mouse Epidermis or Depletion in Keratinocytes Disrupts Tight Junctions and the Permeability Barrier

(A–C) Immunostaining for Occludin (A), ZO-1 (B), and Claudin-4 (C) in *Esrp1*$^{-/-}$;*Esrp2*$^{-/-}$DKO (double knockout) and control *Esrp1*$^{+/+}$;*Esrp2*$^{-/-}$ epidermis showing disrupted Occludin continuity at the stratum granulosum (SG) layer. DAPI (blue).

(C) Claudin-4 staining showing reduced thickness of DKO epidermis compared to the control.

(D) Immunofluorescence localization of tight junction (TJ) markers in the mouse MKC-6 keratinocytes cell line 96 hr after a calcium shift. Analysis was done in cells transduced with a control non-targeting shRNA or shRNAs targeting *Esrp1* and *Esrp2*.

(E) Schematic representing the paracellular biotin permeability assay.

(F) Control (Esrp1$^{+/+}$;Esrp2$^{-/-}$) or Esrp DKO (Esrp1$^{-/-}$;Esrp2$^{-/-}$) E18.5 mouse embryo skin injected intradermally with biotin was stained with streptavidin to follow the penetration of biotin (green) and counterstained with TJ marker Occludin (red) and DAPI (blue) to mark the TJs in the SG layer.

Author Manuscript Author Manuscript Author Manuscript Author Manuscript

(G and H) Transepithelial electrical resistance (TEER) was measured across confluent control, *Esrp1*, *Esrp2*, or *Esrp1/2* shRNA knockdown MKC-6 keratinocyte cell monolayers stimulated with calcium for the indicated times suing Esrp1 shRNA#1 (G) and Esrp1 shRNA#2 (H). (G) and (H) used different Esrp1 shRNAs. Tracer flux of 4kDa FITC-dextran in control or *Esrp* depleted keratinocyte cells is indicated as percent tracer flux relative to a transwell with no cells.

Error bars indicate means ± SDs, n = 3. Statistical significance comparing each group with control was determined by t test. *$p < 0.05$, **$p < 0.005$, ****$p < 0.0001$.

Author Manuscript Author Manuscript Author Manuscript Author Manuscript

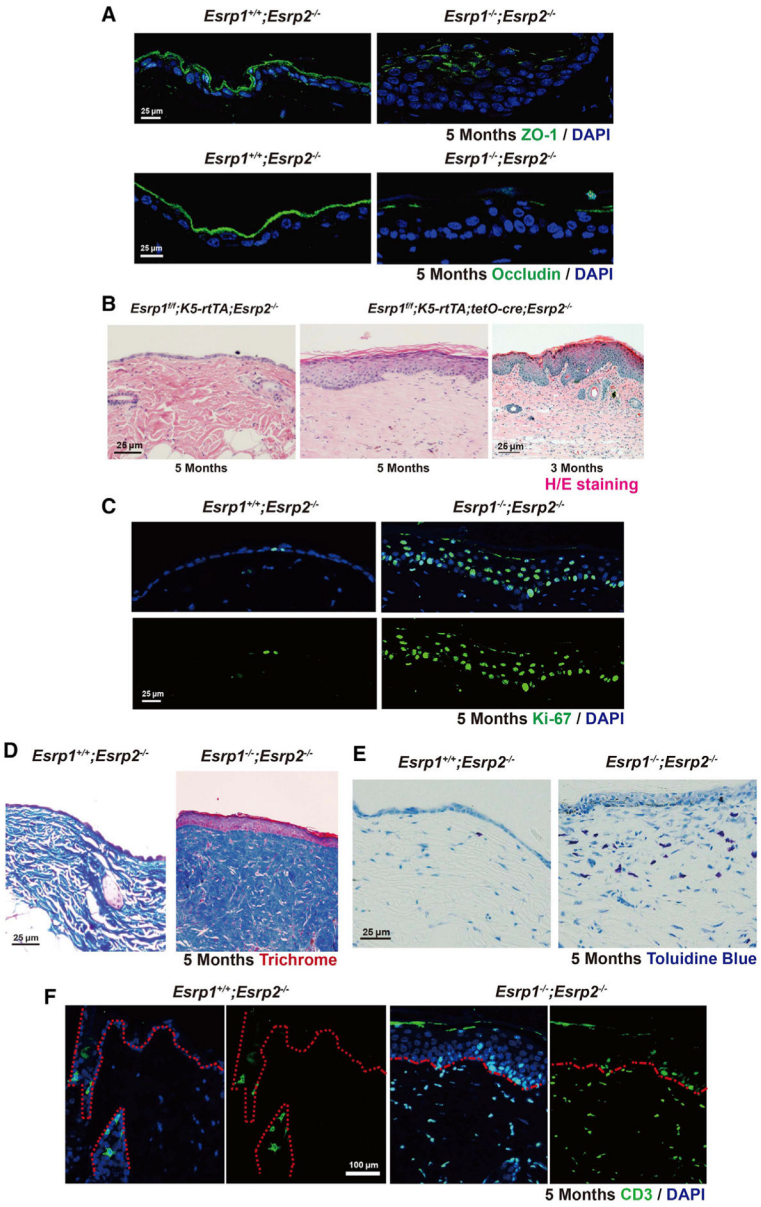

Figure 2. Postnatal Induction of Esrp Ablation in the Epidermis Leads to Disrupted TJ, Epidermal Thickening, Inflammation, and Scarring

(A) Control (*Esrp1*$^{f/f}$*; K5-rtTA;Esrp2*$^{-/-}$) or Esrp DKO (*Esrp1*$^{f/f}$*; K5-rtTA;tetO-Cre;Esrp2*$^{-/-}$) 5-month-old skin immunostained for ZO-1 and Occludin (green).

(B) Longitudinal paraffin section from mice back skin of control and *Esrp1*$^{f/f}$*; K5-rtTA;tetO-Cre;Esrp2*$^{-/-}$ mice. H&E stain reveals that Esrp ablation causes hyperthickening of the epidermis.

(C) Ki-67 proliferation assay. Ki-67^{+}cells (green) and DAPI (blue).

(D) Masson's trichrome stain indicates a high amount of collagen deposition and fibrosis in Esrp DKO epidermis.

(E) Toluidine blue stain shows an increased number of mast cells (dark blue) in Esrp DKO dermis compared to control.

Author Manuscript Author Manuscript Author Manuscript Author Manuscript

(F) Immunofluorescence of cytokine marker CD3 (green) showed increased $CD3^+$in the Esrp DKO dermis.

Author Manuscript Author Manuscript Author Manuscript Author Manuscript

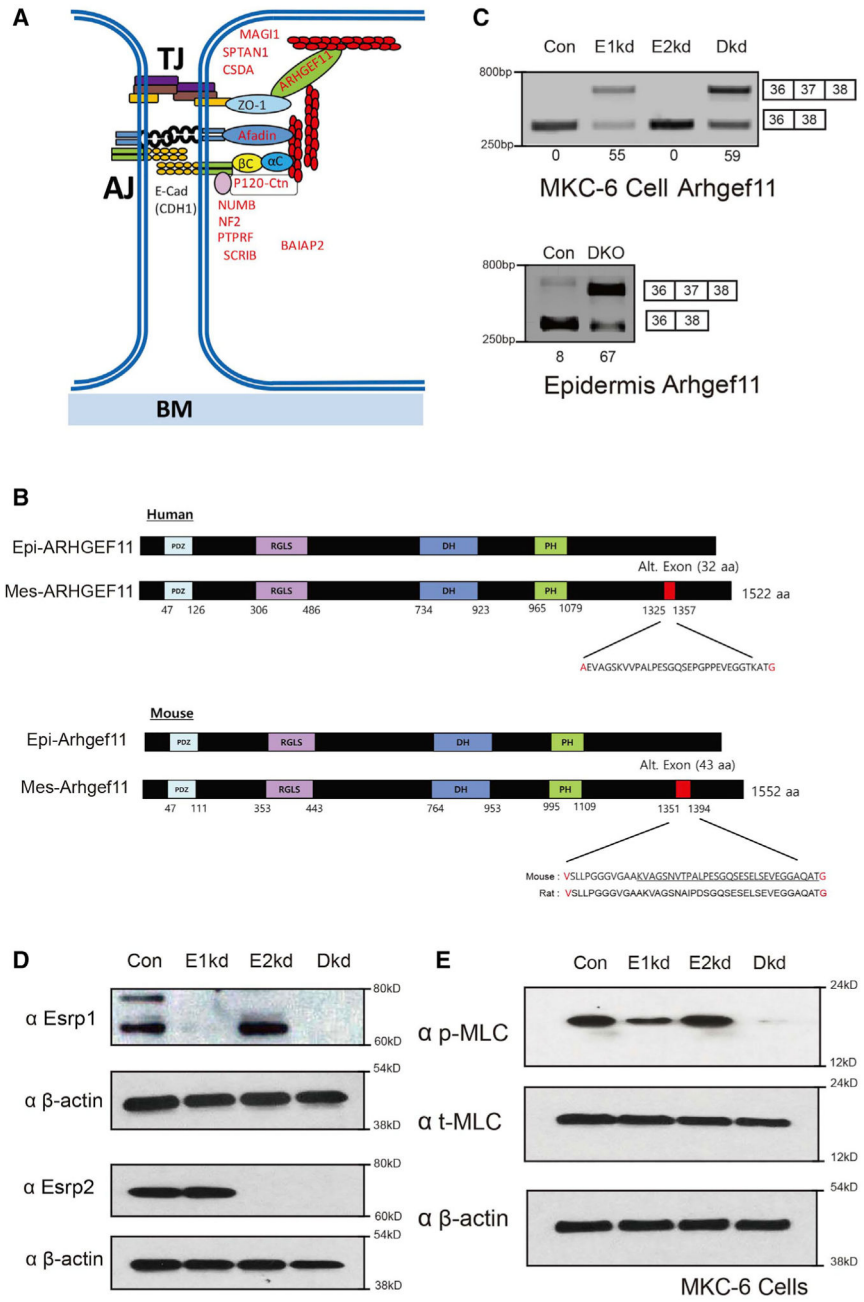

Figure 3. Depletion of Esrp1 and Combined Depletion of Esrp1 and Esrp2 Leads to Progressive Reduction in Phosphorylation of Myosin Light Chain in Keratinocytes

(A) Schematic of proteins encoded by alternative splicing targets of Esrps that are associated with tight junctions and/or adherens junctions.

(B) Schematic of human and mouse Arhgef11 epithelial and mesenchymal protein isoforms resulting from inclusion of or skipping exon 37. The amino acid positions are indicated along with the sequence encoded by the alternative exon. The mouse and rat amino acid sequences are underlined to indicate the similar 32 amino acids in human and rodent isoforms, in which the additional upstream 11 amino acids result from the use of an

Author Manuscript Author Manuscript Author Manuscript Author Manuscript

upstream 3′ splice site in the mouse sequence compared to the human gene. Amino acids in red indicate those that differ, depending on whether the exon is spliced or skipped.

(C) RT-PCR analysis of Arhgef11 exon 37 splicing in control Kd, *Esrp1* Kd, *Esrp2* Kd, and combined *Esrp1;Esrp2* Kd cells. Values for exon 37 percentage spliced in (PSI) are indicated beneath each lane. Also seen is RT-PCR showing increased exon splicing in *Esrp1*$^{-/-}$;*Esrp2*$^{-/-}$epidermis compared to control wild-type epidermis.

(D) Western blot validation of knockdown efficiency.

(E) Reduced phosphorylation of myosin light chain (MLC) in MKC-6 cells depleted for Esrp1, and combined Esrp1;Esrp2 ablation compared to control or Esrp2 depleted cells by immunoblotting.

Author Manuscript Author Manuscript Author Manuscript Author Manuscript

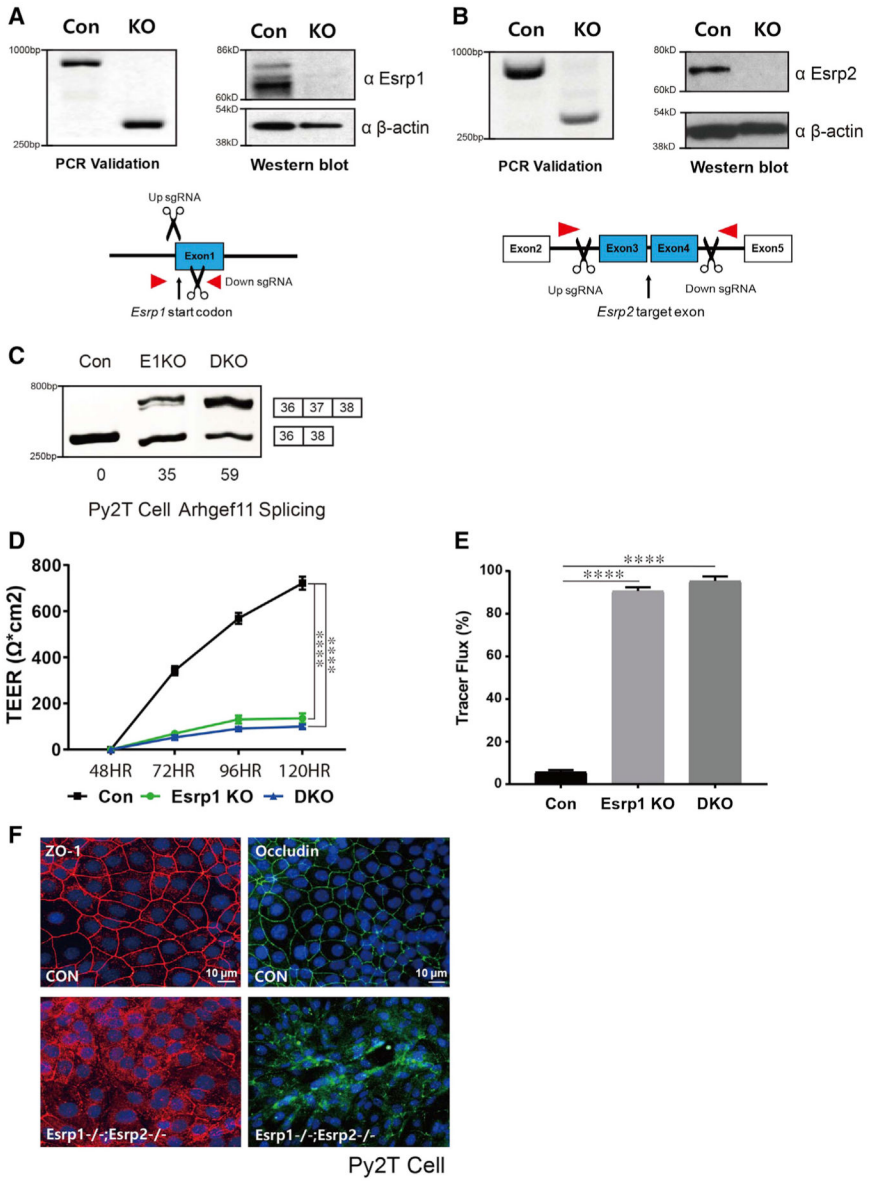

Figure 4. Generation of CRISPR/Cas9-Mediated Esrp KO in Epithelial Cells

(A and B) Schematics and validation using CRISPR/Cas9 to ablate *Esrp1* (A) and *Esrp2* (B) in Py2T cells at the level of genomic DNA and protein by western blot. For Esrp1, a Cas9 nickase strategy was used to target the Esrp1 start codon region, whereas standard Cas9 was used to delete exons in Esrp2 that would disrupt the reading frame.

(C) RT-PCR analysis of Arhgef11 exon 37 splicing in control, *Esrp1*$^{-/-}$ knockout (KO), *Esrp1*$^{-/-}$; *Esrp2*$^{-/-}$ DKO Py2T cells. Values for exon 37 percentage spliced in (PSI) are indicated beneath each lane.

(D) TEER was measured across confluent control or KO epithelial cell monolayers that had been stimulated with calcium for the indicated times.

Author Manuscript Author Manuscript Author Manuscript Author Manuscript

(E) FITC-dextran tracer flux of control, *Esrp1* KO, or *Esrp1/2* DKO epithelial cells. Error bars indicate means ± SDs, n = 3. Statistical significance comparing each group with control was determined by t test. ****$p < 0.0001$.

(F) Disrupted Occludin localization in *Esrp1*$^{-/-}$;*Esrp2*$^{-/-}$ DKO Py2T epithelial cells after Ca^{2+} switch.

Author Manuscript Author Manuscript Author Manuscript Author Manuscript

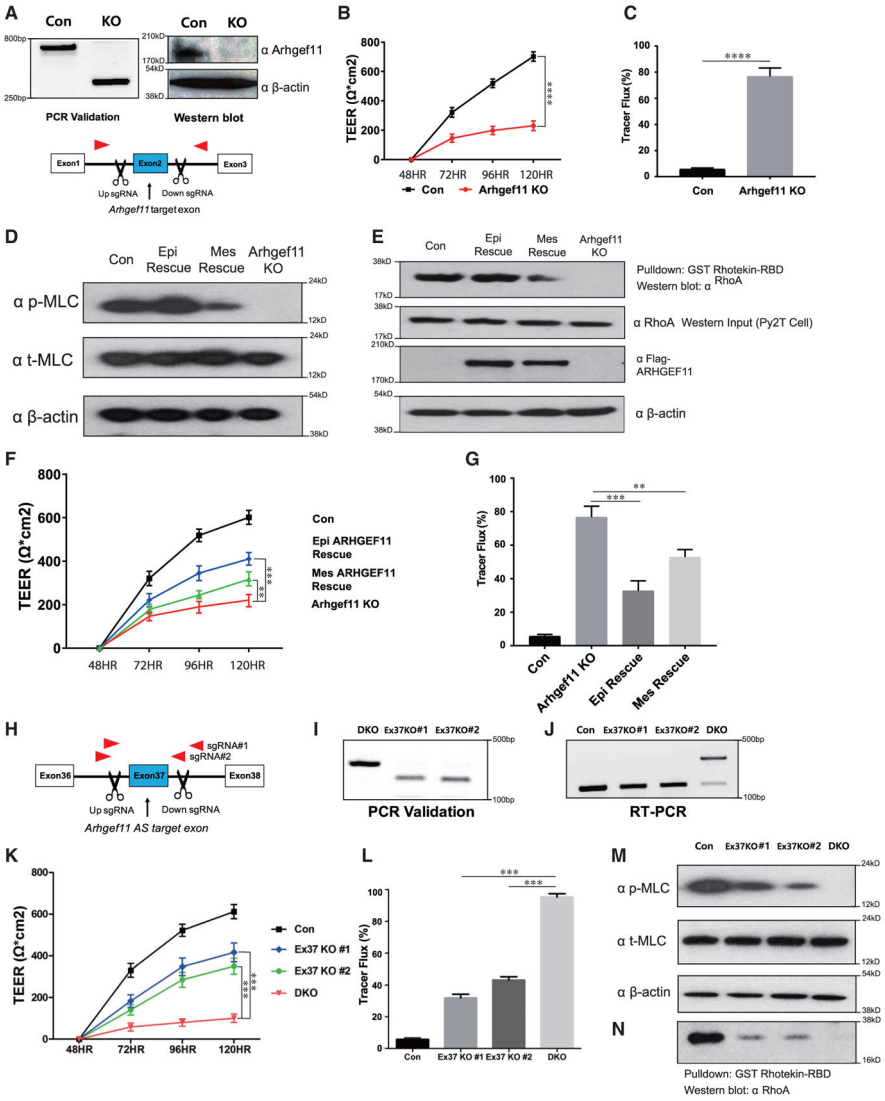

Figure 5. Epithelial ARHGEF11 Isoforms Preferentially Rescue MLC Phosphorylation and Tight Junction Function in Arhgef11 KO Epithelial Cells

(A) Schematics and validation using CRISPR/Cas9 to ablate *Arhgef11* in Py2T cells at the level of genomic DNA and protein by western blot.

(B and C) TEER (B) and FITC-dextran tracer flux (C) in control or *Arhgef11* KO epithelial cell monolayers after calcium switch. Error bars indicate means ± SDs, n = 3. Statistical significance comparing each group with control was determined by t test. ****$p < 0.0001$.

(D) Immunoblot showing that transfection of a cDNA for the epithelial ARHGEF11 isoform rescue (Epi Rescue) restores phosphorylation of MLC in *Arhgef11* KO Py2T cells, whereas a cDNA encoding the mesenchymal ARHGEF11 isoform (Mes Rescue) shows reduced recovery.

(E) RhoA activity assay (Rhotekin assay) showing a higher level of active RhoA GTP in KO cells rescued with the epithelial isoform compared to the mesenchymal isoform. Equal levels of total RhoA are indicated by western blot. Immunoblot showing equal Epi- and Mes-ARHGEF11 protein expression in transfected Py2T cells.

Author Manuscript Author Manuscript Author Manuscript Author Manuscript

(F and G) TEER (F) and FITC-dextran flux (G) assay shows greater rescue with the epithelial ARHGEF11 isoform compared to the mesenchymal isoform. Error bars indicate means ± SDs, n = 3. Statistical significance comparing Epi and Mes Rescue with ARHGEF11KO was determined by t test. **$p < 0.005$; ***$p < 0.001$.

(H) Schematic of CRISPR/Cas9 strategy to ablate Arhgef11 alternative splicing (AS) exon37 in *Esrp1;Esrp2* DKO Py2T cells using 2 different sgRNA pairs.

(I and J) Validation of exon 37 deletion in genomic DNA by PCR (I) and restoration of the epithelial pattern of Arhgef11 splicing by RT-PCR (J).

(K and L) TEER (K) and FITC-dextran flux (L) assays showing partial rescue of tight junction integrity with conversion of endogenous Arhgef11 from predominantly the mesenchymal-to-epithelial pattern in *Esrp1;Esrp2* DKO cells. Error bars indicate means ± SDs, n = 3. Statistical significance comparing exon 37 deletion in DKO cells was determined by t test. ***$p < 0.001$.

(M) Deletion of *Arhgef11* exon 37 partially rescues MLC phosphorylation in *Esrp1;Esrp2* DKO Py2T cells.

(N) RhoA activity assays showing that deletion of *Arhgef11* exon 37 partially restores RhoA activation in *Esrp1;Esrp2* DKO cells.

Author Manuscript Author Manuscript Author Manuscript Author Manuscript

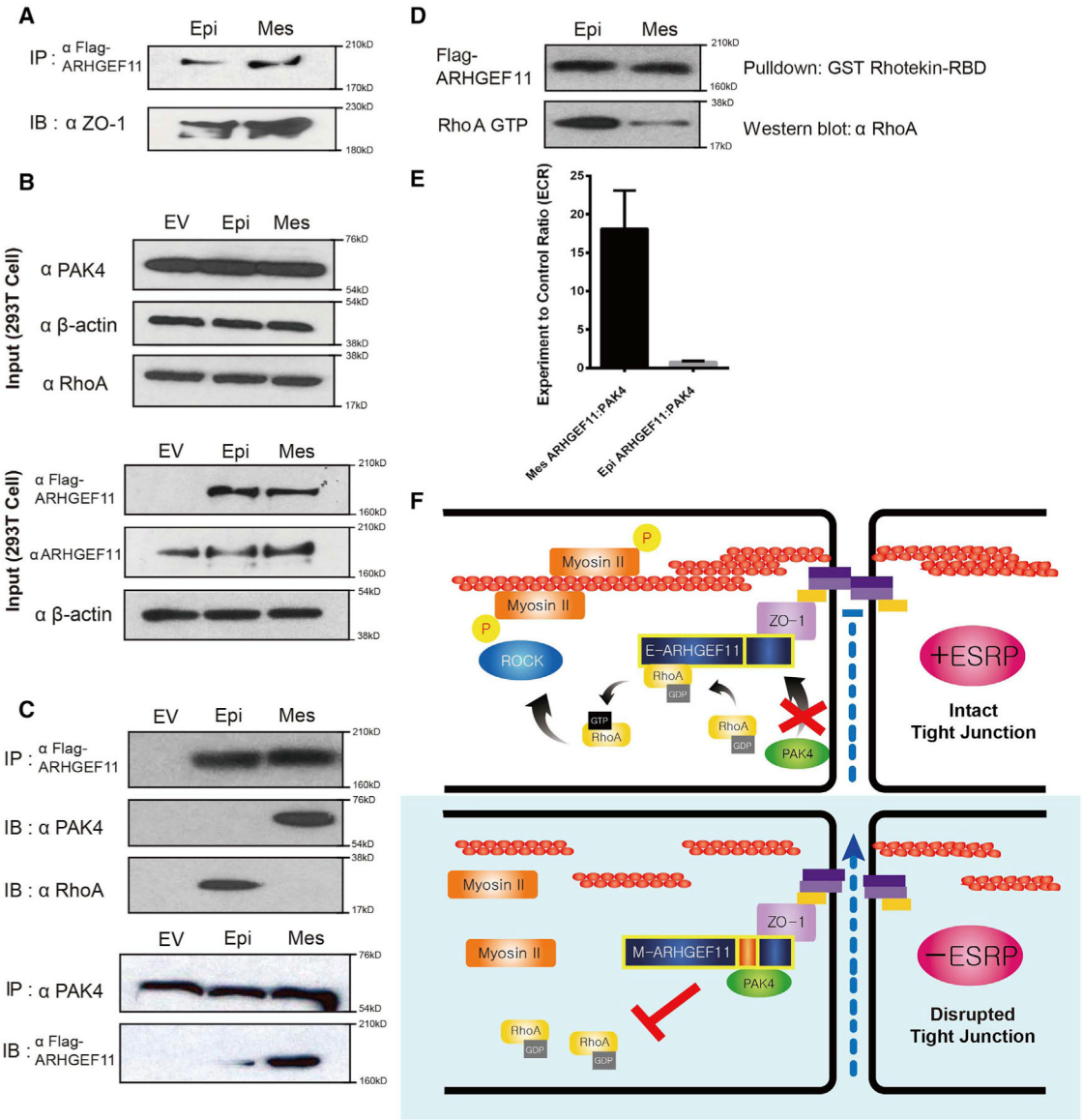

Figure 6. Differential Binding of the Mesenchymal Isoform of ARHGEF11 to Inhibitory PAK4 Leads to Reduced RhoA Activation Compared to the Epithelial Isoform

(A) FLAG-Arhgef11 isoforms transfected in 293T cells were immunoprecipitated with anti-FLAG antibodies and immunoblotted for ZO-1, demonstrating equivalent ZO-1 binding.

(B) Western immunoblots showing levels of the indicated proteins in input samples.

(C) Transfected FLAG-Arhgef11 isoforms were immunoprecipitated with anti-FLAG antibodies and immunoblotted for p21-activated kinase 4 (PAK4) and RhoA. Immunoprecipitation of endogenous PAK4 confirms preferential binding to the mesenchymal ARHGEF11 isoform.

(D) RhoA activity assay reveals that Epi-Arhgef11 more efficiently activates RhoA than Mes-Arhgef11 when overexpressed in 293T cells.

(E) The mesenchymal but not the epithelial isoform of ARHGEF11 binds to PAK4 in the MAPPIT assay. The experimental-to-control ratio (ECR) is calculated from luciferase

Author Manuscript Author Manuscript Author Manuscript Author Manuscript

readings as outlined in Method Details. Error bar represents SD. Experiments were performed in triplicate.

(F) Schematic of model by which the epithelial isoform of ARHGEF11 maintains the PJAR as a result of reduced binding to inhibitory PAK4.

Author Manuscript Author Manuscript Author Manuscript Author Manuscript

KEY RESOURCES TABLE

REAGENT or RESOURCE	SOURCE	IDENTIFIER
Antibodies		
ZO-1	Invitrogen	Cat#40-2200; RRID: AB_2533456
Claudin-1	Invitrogen	Cat#71-7800; RRID: AB_2533997
PAK4	Cell Signaling	Cat#3242S; RRID: AB_2158622
phospho-MLC2	Cell Signaling	Cat#3675S; RRID: AB_2250969
MLC2	Cell Signaling	Cat#3672S; RRID: AB_10692513
FLAG-M2	Sigma	Cat#F1804; RRID: AB_262044
β-actin	Sigma	Cat#A2228; RRID: AB_746697
Occludin	Life technologies	Cat#331-500; RRID: AB_2533101
Rabbit IgG Alexa 488	Life technologies	Cat#A24922; RRID: N/A
Mouse IgG Alexa 594	Life technologies	Cat#A24921; RRID: AB_2536036
Streptavidin, Alexa 488	Life technologies	Cat#S32354; RRID: N/A
PDZ-RhoGEF(ARHGEF11)	BethylLaboratorues	Cat#A301-952A; RRID: AB_1548009
RhoA	Cytoskeleton	Cat#ARH04; RRID: N/A
Esrp1	(Warzecha et al., 2010)	N/A
Esrp2	This paper	N/A
CD3	Abcam	Cat#5690; RRID: AB_305055
F4/80	Abcam	Cat#6640; RRID: AB_1140040
Chemicals, Peptides, and Recombinant Proteins		
EZ-Link sulfo-NHS-LC-biotin	Thermo Scientific	Cat#21327
Lipofectamine 3000	Invitrogen	Cat#11668019
Bovine Serum Albumin	Cell Signaling	Cat#9998S
T4 DNA Ligase	Biolab	Cat#M0202S
3X FLAG peptide	Sigma	Cat#F3290
Protein A Agarose	Invitrogen	Cat#15918-014
Random hexamers	Thermo	SO142
M-MLV Reverse Transcriptase	Promega	M170A
Prolong Gold antifade reagent with DAPI	Invitrogen	Cat#P36935
Anti-FLAG Affinity Gel	Sigma	Cat#A2220
TransIT-293	Mirus	Cat#MIR2700
Critical Commercial Assays		
Rho Activation Assay Biochem Kit	Cytoskeleton	Cat#BK036
Millicell® ERS-2 Voltohmmeter	Millipore	Cat#MERS0002
Experimental Models: Cell Lines		
MKC-6	(Troy and Turksen, 1999)	N/A
293T	ATCC	CRL-3216

Author Manuscript Author Manuscript Author Manuscript Author Manuscript

REAGENT or RESOURCE	SOURCE	IDENTIFIER
Py2T	Gerhard Christofori (Waldmeier et al., 2012)	N/A
Experimental Models: Mice Strains		
Esrp1$^{-/-}$;*Esrp2*$^{-/-}$	(Bebee et al., 2015)	N/A
Esrp1$^{-/-}$;*Esrp2*$^{+/+}$	(Bebee et al., 2015)	N/A
Esrp1$^{f/f}$;*Esrp2*$^{-/-}$;*K5-rtTA;tetO-Cre*	This paper	N/A
Tg(tetO-cre)1Jaw/J (tetO-Cre)	The Jackson Laboratory	JAX stock #006224
Keratin 5-rtTA (K5-rtTA)	Sarah Millar (Penn)	(Diamond et al., 2000)
Oligonucleotides		
Primers for amplification of hEpi-ARHGEF11 cDNA for recombinant protein expression Forward:	This paper	N/A
GGGAATTCGCCACCATGAGTGTAAGGTTACCCCA		
Primers for amplification of hEpi-ARHGEF11 cDNA for recombinant protein expression Reverse:	This paper	N/A
GGGCGGCCGCTGGTCCTGGTGACGCGGCTG		
Primers for amplification of mEpi-Arhgef11 cDNA for recombinant protein expression Forward:	This paper	N/A
GGGAATTCGCCACCATGAGTGTAAGGTTACCCCA		
Primers for amplification of mEpi-Arhgef11 cDNA for recombinant protein expression Reverse:	This paper	N/A
GGGCGGCCGCTGGTCCTGGTGACGCGGCTG		
Arhgef11 and ARHGEF11 RT-PCR Forward:	This paper	N/A
TCAAGCTCAGAACCAGCAGGAAGT		
Arhgef11 and ARHGEF11 RT-PCR Reverse:	This paper	N/A
TGCTCGATGGTGTGGAAGATCACA		
Single-guide RNA Sequences, see Table S1	This paper	N/A
PCR primer sequences used to confirm CRISPR/Cas9 mediated KO, see Table S2	This paper	N/A
shRNA sequences used for Esrp1 or Esrp2 knock down experiments, see Table S3	This paper	N/A
Recombinant DNA		
psPAX2	Addgene	Addgene#12260
pCMV-VSV-G	Addgene	Addgene#8454
Plasmid: pSg-Puro	This paper	N/A
Plasmid: pLKO.1-puro	Sigma	#SHC001
Plasmid: pIBX-Epi-Arhgef11	This paper	N/A
Plasmid: pIBX-Mes-Arhgef11	This paper	N/A
Plasmid: pIPX-Epi-ARHGEF11	This paper	N/A
Plasmid: pIPX Mes-ARHGEF11	This paper	N/A
Plasmid: pIBX-Epi-ARHGEF11	This paper	N/A
Plasmid: pIBX-Mes-ARHGEF11	This paper	N/A
Plasmid: pIBX-Cas9	This paper	N/A

Author Manuscript Author Manuscript Author Manuscript Author Manuscript

REAGENT or RESOURCE	SOURCE	IDENTIFIER
Plasmid: PX330	Addgene	Addgene#42230
ARHGEF11 cDNA	Dharmacon	BC057394
Arhgef11 cDNA	Dharmacon	BC079565
Plasmid: pMG1-SVT	(Eyckerman et al., 2001)	N/A
Plasmid: pSEL+2L-hMal	(Eyckerman et al., 2001)	N/A
Plasmid: pMG1-GW	(Eyckerman et al., 2001)	N/A
Plasmid: pSEL+2L-GW	(Eyckerman et al., 2001)	N/A
Plasmid: pXP2d2-rPAP1-luci	(Eyckerman et al., 2001)	N/A
Software and Algorithms		
Prizm	Graphpad	N/A
ImageQuant TL, version 7.0	GE Healthcare	N/A